

**INVESTIGATION ON PERFORMANCE OF
DIRECT CONTACT MEMBRANE
DISTILLATION UNDER DIFFERENT CHANNEL
DESIGNS**

HUANG KEE KEE

UNIVERSITI TUNKU ABDUL RAHMAN

**INVESTIGATION ON PERFORMANCE OF DIRECT CONTACT
MEMBRANE DISTILLATION UNDER DIFFERENT CHANNEL
DESIGNS**

HUANG KEE KEE


**A project report submitted in partial fulfilment of the
requirements for the award of Bachelor of Mechanical
Engineering with Honours**

**Lee Kong Chian Faculty of Engineering and Science
Universiti Tunku Abdul Rahman**

September 2024

DECLARATION

I hereby declare that this project report is based on my original work except for citations and quotations which have been duly acknowledged. I also declare that it has not been previously and concurrently submitted for any other degree or award at UTAR or other institutions.

Signature : 

Name : Huang Kee Kee

ID No. : 2006061

Date : 29 September 2024

APPROVAL FOR SUBMISSION

I certify that this project report entitled **“INVESTIGATION ON PERFORMANCE OF DIRECT CONTACT MEMBRANE DISTILLATION UNDER DIFFERENT CHANNEL DESIGNS”** was prepared by **Huang Kee Kee** has met the required standard for submission in partial fulfilment of the requirements for the award of Bachelor of Mechanical Engineering with Honours at Universiti Tunku Abdul Rahman.

Approved by,

Signature

:



Supervisor

:

Mr. Cheong Wen Chiet

Date

:

29 September 2024

The copyright of this report belongs to the author under the terms of the copyright Act 1987 as qualified by Intellectual Property Policy of Universiti Tunku Abdul Rahman. Due acknowledgement shall always be made of the use of any material contained in, or derived from, this report.

© 2024, Huang Kee Kee. All right reserved.

ACKNOWLEDGEMENTS

I would like to thank everyone who had contributed to the successful completion of this project. I would like to express my gratitude to my previous research supervisor, Mr. Lee Sze Shin, and my current research supervisor, Mr. Cheong Wen Chiet, for their invaluable advice, guidance, and enormous patience throughout the development of the research.

In addition, I would also like to express my gratitude to my loving parents and friends who had helped and given me encouragement.

ABSTRACT

Freshwater is essential for all living organisms, serving as a fundamental requirement for biological processes. Addressing the increased demand for freshwater or its scarcity can be achieved through desalination processes, such as membrane distillation (MD), which desalts seawater. This study investigates the impact of different channel designs on the performance of Direct Contact Membrane Distillation (DCMD) systems. It was found that a channel with a higher channel height yields better performance and achieves optimal results when the channel height is close to the optimum. However, further increases in channel height beyond the optimum lead to a decline in performance. Similarly, for the fin-to-channel width ratio, a decrease in the ratio yields better performance, with the best results obtained when the ratio is close to the optimum. Further decreases in the ratio beyond the optimum also lead to a decline in performance. Furthermore, a channel design with fewer fins was found to have worse performance compared to a design with more fins. Therefore, a channel design with a channel height of 1.6 mm, a channel width of 2.6 mm, a fin width of 2.13 mm, and a total of 9 fins, which is close to the optimum, provides the best performance results, with an average permeate flux of 4.92 g/(m²s) and a 32.8% improvement in the DCMD process.

TABLE OF CONTENTS

DECLARATION		i
APPROVAL FOR SUBMISSION		ii
ACKNOWLEDGEMENTS		iv
ABSTRACT		v
TABLE OF CONTENTS		vi
LIST OF TABLES		viii
LIST OF FIGURES		ix
LIST OF SYMBOLS / ABBREVIATIONS		xi
LIST OF APPENDICES		xii
 CHAPTER		
1	INTRODUCTION	1
	1.1 General Introduction	1
	1.2 Importance of the Study	4
	1.3 Problem Statement	5
	1.4 Aim and Objectives	5
	1.5 Scope and Limitation of the Study	6
	1.6 Contribution of study	6
	1.7 Outline of the Report	6
2	LITERATURE REVIEW	8
	2.1 Introduction to Literature Review	8
	2.2 Effect of Flow Configurations on DCMD Performance	8
	2.3 Effect of Feed and Permeate Channels' Height on DCMD Performance	10
	2.4 Effect of Surface Roughness on DCMD Performance	11
	2.5 Effect of Spacer on DCMD Performance	14

2.6	Effect of Multiple Channels Module on DCMD Performance	21
2.7	Summary	22
3	METHODOLOGY AND WORK PLAN	23
3.1	Introduction	23
3.2	Flowchart	23
3.3	Experimental Setup	25
3.4	Experimental Procedure	26
3.5	Parameters for the Proposed Study	27
3.6	Parameters Tested in the Experiment	29
3.7	Design of Finned Blocks	29
3.8	Fabrication Process for Finned Blocks	34
3.9	Gantt chart	38
3.10	Summary	39
4	RESULTS AND DISCUSSION	40
4.1	Introduction	40
4.2	Relationship between temperature differences and water production rates for a DCMD module with various channel designs.	41
4.3	Relationship between channel height and the fin-to-channel width ratio in relation to the improvement in water production rate	46
4.4	Relationship between the number of fins and the water production rate	53
4.5	Conductivity Test for the DCMD Experiment	58
4.6	Summary	60
5	CONCLUSIONS AND RECOMMENDATIONS	61
5.1	Conclusions	61
5.2	Recommendations for future work	62
	REFERENCES	63
	APPENDICES	66

LIST OF TABLES

Table 3.1:	Experimental parameters for the proposed study	28
Table 3.2:	Design parameters for the proposed study	28
Table 3.3:	Specifications for all block designs.	34
Table 4.1:	Types of blocks used.	42
Table 4.2:	Comparison of the average permeate fluxes for different channel heights and fin-to-width ratios.	47
Table 4.3:	Comparison of the percentage increase in average permeate flux compared to the flat block for various channel heights and fin-to-width ratios.	48
Table 4.4:	Specifications for 9-fin, 8-fin and 7-fin blocks.	53
Table 4.5:	Comparison of the average permeate fluxes for blocks with different numbers of fins.	55
Table 4.6:	Comparison of the percentage increase in average permeate flux compared to the flat block for different numbers of fins.	56
Table 4.7:	Conductivity of the permeate solution before and after the experiment, with rejection rates for each block type.	59

LIST OF FIGURES

Figure 1.1:	Basic operating principles of MD process (Shirazi and Kargari, 2015).	2
Figure 1.2:	Four primary configurations of MD process (Ashoor, et al., 2016).	3
Figure 3.1:	Flowchart of the overall process.	24
Figure 3.2:	Schematic Diagram of the DCMD experimental setup.	25
Figure 3.3:	Actual DCMD experimental setup.	25
Figure 3.4:	Assembly of DCMD module.	27
Figure 3.5:	Permeate conductivity measurement using conductivity meter.	27
Figure 3.6:	Locations of parameters H, W, and W_f in the channel design.	29
Figure 3.7:	Drawing of the flat block design.	30
Figure 3.8:	Drawing of the Type 1 finned block design.	30
Figure 3.9:	Drawing of the Type 2 finned block design.	31
Figure 3.10:	Drawing of the Type 3 finned block design.	31
Figure 3.11:	Drawing of the Type 4 finned block design.	32
Figure 3.12:	Drawing of the Type 5 finned block design.	32
Figure 3.13:	Drawing of the Type 6 finned block design.	33
Figure 3.14:	Drawing of the 8-fin finned block design.	33
Figure 3.15:	Drawing of the 7-fin finned block design.	34
Figure 3.16:	Aluminum as raw material for block fabrication.	36
Figure 3.17:	Cutting aluminum using a band saw cutter.	36
Figure 3.18:	Milling of aluminum block to desired dimensions using a milling machine.	36
Figure 3.19:	Inserting G-code into the CNC control panel.	37

Figure 3.20:	CNC milling of channels on the block.	37
Figure 3.21:	Fabricated finned block samples.	37
Figure 3.22:	Gantt chart for FYP 1.	38
Figure 3.23:	Gantt chart for FYP 2.	39
Figure 4.1:	Permeate flux in every 10 minutes plotted against the temperature difference for the flat block and types 1 to 6 blocks.	43
Figure 4.2:	Permeate flux plotted against time for the flat block and types 1 to 6 blocks.	44
Figure 4.3:	Average permeate flux for blocks with different channel heights.	47
Figure 4.4:	Average permeate flux for blocks with different fin-to-width ratios.	48
Figure 4.5:	Percentage increase in average permeate flux for blocks with different channel heights.	49
Figure 4.6:	Percentage increase in average permeate flux for blocks with different fin-to-width ratios.	49
Figure 4.7:	Permeate flux in every 10 minutes plotted against the temperature difference for the 9-fin, 8-fin, and 7-fin blocks.	54
Figure 4.8:	Permeate flux plotted against time for the 9-fin, 8-fin, and 7-fin blocks.	54
Figure 4.9:	Average permeate flux of blocks with different numbers of fins.	56
Figure 4.10:	Percentage increase in average permeate flux compared to the flat block with different numbers of fins.	57

LIST OF SYMBOLS / ABBREVIATIONS

1D	one-dimensional
2D	two-dimensional
3D	three-dimensional
AGMD	air gap membrane distillation
CFD	computational Fluid Dynamics
DCMD	direct contact membrane distillation
H	channel height, mm
H/W	channel height-to-width ratio
MD	membrane distillation
RO	reverse osmosis
SGMD	sweep gas membrane distillation
T_f	feed temperature, °C
T_p	permeate temperature, °C
VMD	vacuum membrane distillation
W	channel width, mm
W_f/W	fin-to-channel width ratio
W_f	fin width, mm

LIST OF APPENDICES

Appendix A: Experimental Data	66
-------------------------------	----

CHAPTER 1

INTRODUCTION

1.1 General Introduction

As the global population continues to grow in this modern era, the demand for fresh water is increasing rapidly. Although nearly 70 percent of the Earth's surface is covered by water, not all this water can be consumed by humans. This is because nearly 97.5 percent of the water on Earth is seawater, while the total amount of available fresh water is only around 2.5 percent. In fact, the fresh water that is readily available and accessible for human consumption, agriculture, industry, and other uses is only around 0.5 percent, while the remaining portion of fresh water is mostly in the form of glaciers, ice caps, and permanent snow-covered regions like the Arctic and Antarctic, which cannot be used immediately by humans. Freshwater is always the basic need for all living organisms to carry out biological processes. Due to the increased number of factories leading to increased pollution and the increased number of populations leading to increased demand for fresh water, the scarcity of freshwater resources has become a critical issue and concern nowadays. Therefore, the improvement in desalination technologies is extremely important nowadays as it can help to mitigate this issue by producing fresh water from seawater or saltwater (Sampaio, et al., 2023; Shirazi and Kargari, 2015).

Desalination is a relatively low-cost method that may be used to solve the scarcity of freshwater issue by removing salts and impurities from seawater. There are several techniques available for the desalination process in the world, with the two most basic approaches being ordinary distillation and membrane desalination. In membrane desalination methods, reverse osmosis (RO) is one of the most widespread and typical kinds of isothermal desalination technologies that are extensively researched by many researchers. However, there is actually another non-isothermal membrane desalination process that might not be as popular as RO, called membrane distillation (MD). There are various advantages to using MD over RO, with one of the most attractive advantages being that MD is more affordable than RO. As RO is a pressure-driven process, it requires high pumping power, which consumes a lot of energy.

While MD can be carried out under atmospheric pressure, which does not require high pumping power, thereby significantly reducing the energy consumption of the MD process (Momeni, et al., 2024).

MD is a separation process driven by thermal energy that uses a hydrophobic microporous membrane to separate the feed stream (hot side) from the permeate stream (cold side). It is an emerging non-isothermal membrane process that utilizes thermal energy to produce the vapor phase of volatile molecules in the feed stream and condense the permeated vapor in the permeate stream. Therefore, the temperature gradient across the membrane provides the driving force for heat transport, resulting in a vapor pressure difference across the membrane. The water vapor from the feed stream is then transported to the permeate side through the membrane pores. Since the membrane is hydrophobic, it ensures that only vapor can pass through the membrane and no liquid is distilled through it. The main advantage of MD is that distillation can occur below the boiling points of the feed solution, with the feed solution temperature typically ranging between 35°C and 85°C only. Another advantage of MD is that the hydrophobic membrane is not wetted by water due to its operation as a non-isothermal process. MD is also less susceptible to membrane fouling and exhibits high solute rejection when compared to conventional membrane technologies like RO, and it remains unaffected by high osmotic pressure in highly saline feed solutions (Ashoor, et al., 2016; Shirazi and Kargari, 2015).

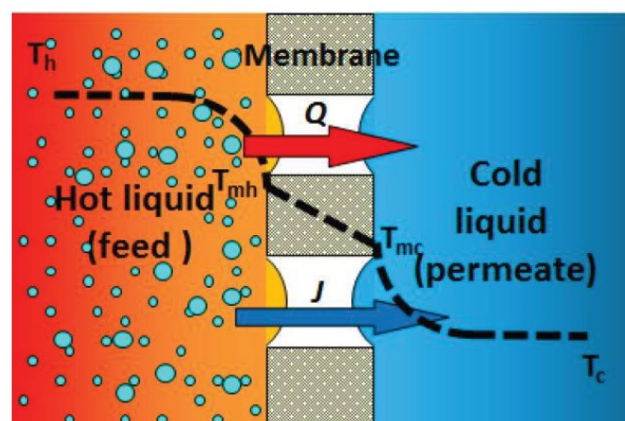


Figure 1.1: Basic operating principles of MD process (Shirazi and Kargari, 2015).

There are four primary configurations for the MD process, which are Direct Contact Membrane Distillation (DCMD), Air-gap Membrane Distillation (AGMD), Sweep Gas Membrane Distillation (SGMD), and Vacuum Membrane Distillation (VMD), as shown in Figure 1.2 (Ashoor, et al., 2016).

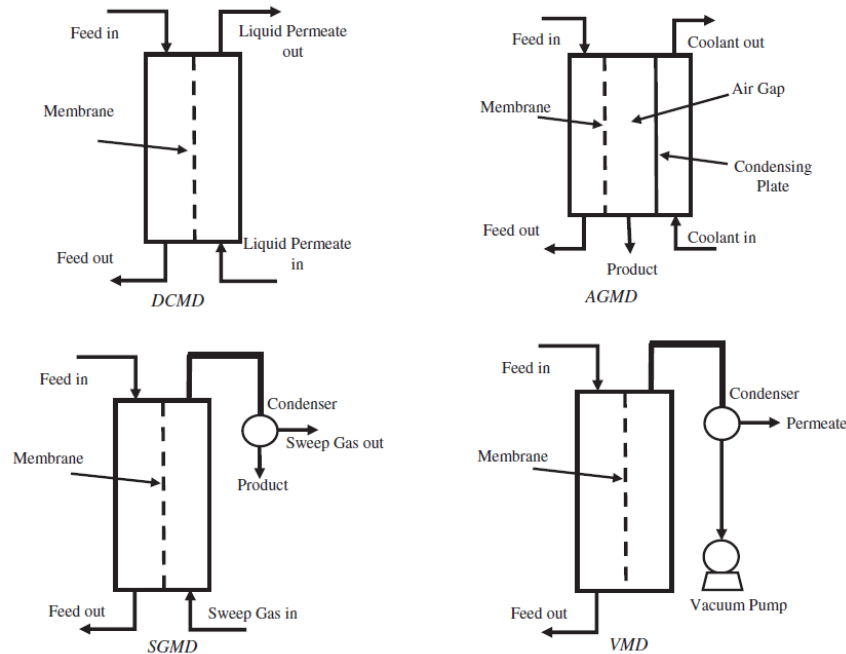


Figure 1.2: Four primary configurations of MD process (Ashoor, et al., 2016).

In this study, DCMD is the primary focus and will be further discussed. DCMD is the simplest and the most popular configuration among others. Unlike other configurations, DCMD involves direct contact between both the hot feed liquid and the cold permeate liquid with the membrane. Therefore, DCMD operates on the fundamental principles of the MD process, in which the hot feed solution is brought into direct contact with the feed side of the membrane, and the cold fluid is brought into direct contact with the permeate side of the membrane. The water vapor on the feed side is then transported to the permeate side through the membrane by the driving force resulting from the temperature gradient. Furthermore, this direct contact mechanism makes the operation of DCMD relatively easy and provides an advantage in obtaining high permeation flux under the correct operating conditions. Nonetheless, DCMD does have its drawbacks compared to other configurations, particularly in terms of thermal energy efficiency, which is lower due to the proximity of the evaporator and

condenser surfaces, resulting in a reduced effective driving force (Ashoor, et al., 2016).

1.2 Importance of the Study

The findings of this study may propose an alternative approach to addressing the challenges encountered by DCMD and offer an evaluation of performance across various channel designs. Most researchers focus on membrane modification methods, such as utilizing nanofiber membranes or decreasing membrane thickness, to enhance DCMD performance. Some researchers also study the use of hollow fibre tubes to enhance DCMD performance, but few have investigated the modification of channel design. Therefore, this study aims to investigate different channel designs and evaluate the effects on fluid flow patterns, heat transfer rates, water production rates, and energy efficiency in DCMD systems. According to World Health Organisation (2023), there are over 2 billion people living in water-stressed countries, a number expected to worsen in some areas due to climate change and a rapidly growing population as of year 2021.

Additionally, in 2022, at least 1.7 billion people worldwide consumed water from sources contaminated with faeces, leading to health problems. Therefore, developing channel designs that enhance DCMD performance can not only aid in seawater desalination but also contribute to industrial wastewater treatment and water purification to address freshwater scarcity issues. Furthermore, advancements in DCMD technology can also benefit industries such as food and beverages, pharmaceuticals, and chemicals by facilitating concentration processes. However, while modifications to channel designs in DCMD systems generally enhance performance by providing thermal stability and consistent efficiency, current DCMD technology still encounters challenges in industrial applications due to issues such as cost, scalability, durability, energy consumption, and process efficiency. Therefore, this study aims to explore how a modification of channel design in the DCMD system could offer improved performance by investigating the effects of different channel designs on water production rates, flow dynamics, and thermal performance.

1.3 Problem Statement

Numerous past studies have shown that the DCMD process using flat channels has been observed to have low efficiency. Therefore, most researchers have proposed different methods or modifications to improve performance by increasing the turbulence effects. One of the methods that can enhance the performance and efficiency of DCMD is by modifying channel designs to increase turbulence effects inside the channels. However, the effectiveness of modifications to channel designs remains uncertain due to insufficient studies comparing the performance of DCMD with different channel designs to the conventional DCMD design, leading to a research gap. The power consumption of the DCMD process using different channel designs is also an important consideration. This is because any change in the channel design may affect the internal transfer profiles inside the DCMD module, which may lead to higher energy requirement and consumption. Another problem that is always a concern in DCMD experiments is the stability of the process. The examples of stability issues are maintaining a consistent temperature gradient across the membrane, reducing membrane fouling and ensuring the durability and long-term performance of the membrane, all of which need improvement today. Additionally, prolonged exposure to high temperatures can lead to membrane degradation, which limits the maximum feed temperature that can be used and reduces the temperature difference, resulting in lower permeate flux. These stability issues will affect the efficiency and reliability of the DCMD process. Therefore, this study aims to enhance the performance and reliability of DCMD systems by investigating how different channel design modifications can increase efficiency, reduce power consumption, and improve system stability.

1.4 Aim and Objectives

The specific aim of this study is to identify the effect of utilizing different channel designs on the performance of DCMD system. The objectives that need to be accomplished to achieve the overall aim in this study are:

- i. To investigate the improvement in water production rates and the effects of temperature differences on the performance of the DCMD module with different channel designs compared to the conventional design.

- ii. To investigate the influence of channel height and the fin-to-channel width (W_f/W) ratio on the performance of the DCMD module with channels having the same height-to-width ratio.
- iii. To investigate the effects of the number of fins on the performance of the DCMD module with channels having the same height and width dimensions.

1.5 Scope and Limitation of the Study

The scope of this study is solely to focus on the impacts of different channel designs on the efficiency and performance of the DCMD process. Other variable parameters or relevant factors are neglected and will not be considered in this study. Despite DCMD being one of the basic membrane distillation methods used in water purification and freshwater production, there is still a scarcity of research studying the performance of DCMD by modifying the channel design, which could be one of the limitations of this study. Furthermore, this study is limited to modifying solely the mechanical component of the channel module, without allowing modifications to the membrane used in the DCMD module.

1.6 Contribution of study

This study contributes to identifying the performance of DCMD systems with the use of different channel designs. The study also provides good suggestions for the channel designs that can enhance fluid flow patterns, heat and mass transfer rates, and water production efficiency in DCMD systems. With this study, researchers in the future can explore the potential application of these channel designs in real-world desalination or water treatment processes.

1.7 Outline of the Report

There are a total of five chapters in this report. Chapter 1 explains the concepts of desalination, the introduction and operating principle of DCMD, the importance of studying DCMD, especially in freshwater production, the challenges faced in DCMD, and the objectives of this research. Next, Chapter 2 discusses the literature review on the parameters related to this study that affect

DCMD performance. Chapter 3 explains the methodology and work plan for conducting the research in this study. Then, Chapter 4 discusses and analyzes the results obtained in this study. Finally, Chapter 5 concludes the findings of this research and gives recommendations for future studies or work in this related field and topic.

CHAPTER 2

LITERATURE REVIEW

2.1 Introduction to Literature Review

In this chapter, the literature review will encompass four main areas focusing on the effect of improvement methods on DCMD performance. Section 2.2 will discuss the effect of surface roughness on DCMD performance. Subsequently, Section 2.3 will explore the effect of channel height on DCMD performance. Following this, Section 2.4 will examine the effect of flow type on DCMD performance. Section 2.5 will analyse the effect of spacers on DCMD performance. Section 2.6 will discuss the effect of multiple channels module on DCMD performance. Finally, Section 2.7 will summarize the literature review.

2.2 Effect of Flow Configurations on DCMD Performance

Ho, et al. (2014) investigated the effect of counter-current flow on flux enhancement in DCMD desalination. To observe the heat and mass transfer of counter-current flow in the DCMD process, the authors conducted experiments with both co-current and counter-current flow setups under same experimental conditions. A theoretical model of the DCMD module was developed to predict the outcomes and trends of the experiment, which were later compared with the experimental results for validation. The experiment included trials using both co-current and counter-current flow DCMD systems, incorporating a range of surface roughness levels, hot fluid temperatures, and fluid flow rates, while maintaining a consistent cold fluid temperature throughout. The experimental results revealed that the productivity of pure water in counter-current flow systems was higher than co-current flow systems due to higher permeation flux of pure water in counter-current flow arrangements. Moreover, the improvement in the temperature polarization coefficient was higher in counter-current flow operation, resulting in higher temperature driving-force on both cold and hot streams compared to co-current flow operation. The experiment also revealed the relationship between fluid flow rate, inlet hot fluid temperature, and pure water flux, indicating that higher hot fluid temperature and larger fluid flow rate correspond to better DCMD module performance and higher pure

water flux. However, excessive fluid flow rates and inlet hot fluid temperatures resulted in a decrease in DCMD module performance in counter-current flow operation. In conclusion, the quantitative consistency between the experimental data and the theoretical predictions in this DCMD system demonstrated the overall reliability of the experimental results.

The study conducted by Park, Norouzi and Park (2019) focused on investigating the impact of different flow configurations on the overall performance of a DCMD system. A two-dimensional (2D) model was developed by the authors based on the experimental module to analyse distilled water production and the thermal performance of the DCMD system with different flow arrangements. The authors utilized ANSYS FLUENT software for Computational Fluid Dynamics (CFD) simulation. Simulations were conducted for both co-current and counter-current flows under the same operating conditions as the reported experiment. The obtained simulation results were then verified and compared with the experimental data collected from the real-world experimental setup to enhance the accuracy and reliability of the simulation results. Relationships between convection thermal resistance, heat flux, and mass flux concerning flow configurations of MD modules were identified during the simulation. Simulation results indicated that the overall convection thermal resistance was lower in the counter-current flow configuration compared to the co-current flow configuration. This was attributed to increased thermal resistance as the flow in the feed and the permeate stream became more developed when passing through the channel. Thus, the mixed inlet and outlet configuration of the counter-current flow led to a more uniform thermal resistance and resulted in lower average thermal resistance compared to co-current flow. Heat flux and mass flux in the counter-current flow configuration were also higher than in the co-current flow configuration. This was because the temperature difference decreased rapidly in co-current flow while remaining nearly constant in counter-current flow when passing through the channel. Therefore, overall distilled water production was higher in the counter-current flow configuration. The authors also conducted simulations with different operating conditions such as varying flow rates and feed temperature to validate and verify the trend of the effect of using both co-current and counter-current flow on DCMD performance. All simulation results

revealed that the performance of the DMCD module with counter-current flow was better than co-current flow. By comparing the simulation results with experimental results, the study demonstrated the reliability and predictive capability of CFD simulations in assessing DCMD performance.

2.3 Effect of Feed and Permeate Channels' Height on DCMD Performance

The study conducted by Rabie, Elkady and El-Shazly (2021) investigated the impact of feed and permeate channels' height on overall DCMD performance. The authors first designed a three-dimensional (3D) model and then introduced it into the software Ansys 2020 for simulation purposes to obtain numerical solutions and observe the optimum operating conditions for the experiment before carrying out the actual experiment. The simulation results were obtained from the Ansys 2020 software and subsequently verified and compared with the experimental data. The experiment was conducted under the same experimental conditions as the simulation but with different channel heights to have fair comparison with the simulation results. The flow rate was varied, and the feed inlet temperature was kept constant throughout the experiment to further validate the trend. The relationship between the heat transfer coefficient, vapor pressure difference, and permeate flux in relation to the channel height was monitored and analysed in the experiment. The experimental results revealed that the overall performance of DCMD improved with decreased channel height for all studied flow rates. This was because decreasing channel height significantly increased the heat transfer coefficient, which reduced temperature polarization effects and brought the membrane surface temperature closer to the corresponding bulk temperature. Additionally, decreasing channel height increased the vapor pressure difference, which increased the driving force and enhanced system performance. Overall, the experimental results were reliable as the experimental results matched perfectly and demonstrated good agreement with the simulation results.

The research conducted by Zare and Kargari (2022) investigated the impact of feed and permeate channels' height on the performance of DCMD desalination systems and determined the optimum channels' height to optimize the DCMD system for achieving the best performance through CFD simulations.

A two-step method was used by the authors to optimize the DCMD system. The authors first developed a 2D CFD model to study the heat and mass transfer in the feed side, membrane side, and permeate side of the DCMD system with counter-current flow. The authors proposed the basic model equations of the feed side, membrane side, and permeate side and solved the equations using COMSOL Multiphase software. Sets of simulation results samples were obtained by the authors by varying the feed velocity and feed temperature to validate the 2D CFD model by comparing the model results with the reported experimental data, ensuring good agreement was achieved to estimate the DCMD system performance properly. The simulation was conducted with different channel heights under the same experimental conditions, keeping the feed and permeate flow rates, permeate temperature, membrane length, and channel length constant throughout the simulation for a fair comparison. The relationship between the heat transfer coefficient, input velocity, and permeate flux in relation to the channel height was monitored and analysed in the simulation. Notably, the simulation results indicated that lower channel heights led to better DCMD performance, showing higher permeate flux and heat transfer coefficients. This was attributed to the higher input velocity at lower channel heights for a constant flow rate, resulting in higher permeate flux and enhanced water flux. Overall, the simulation results were reliable as good agreement was achieved between the reported experimental data and simulation results in this DCMD module.

2.4 Effect of Surface Roughness on DCMD Performance

Chang, et al. (2015) investigated the effects of rough surface channels on DCMD modules through the implementation of CFD simulations. For observing the internal transfer profiles of the MD modules, the Fluent Software was used to simulate the entire DCMD modules with rough surfaces. The simulation results were subsequently verified and compared with the experimental data obtained from the experiment using the R44 channel module. The simulation was run under identical experimental conditions as the DCMD experiment using the R44 channel module to ensure a fair and accurate comparison. A variety of hot fluid temperatures and flow rates were used in both the simulation and the experiment, along with some customized factors including roughness levels and

co- or counter-current flow. The relationships between temperature profiles, mass flux profiles, and heat transfer coefficients to the channel surface roughness of MD modules were monitored and analysed during the simulation. The simulation results indicated that the presence of rough surface in the hot channel caused the thermal entry length in the hot channel to be shorter than in the cold channel. For a co-current flow design, the mass flux was larger solely at the inlet end, but for a counter-current flow configuration, the thermal entrance effects at two channels caused the mass flux to be higher at both ends. Furthermore, in both co- and counter-current flow configurations, the rougher channel module led to larger mass fluxes, which indirectly resulted in higher heat transfer coefficients. In contrast to the co-current flow configuration, the counter-current flow configuration had a greater heat transfer coefficient. Lastly, the simulation results were reliable and closely matched the experimental results in precision.

The study by Chang, Ho and Hsu (2016) investigated the effect of the type of channel surface on heat transfer coefficients in DCMD modules using CFD simulation. To observe transmembrane heat and mass transfer in the DCMD modules, the authors developed a 3D CFD model based on the reported experimental module for simulations, utilizing the Fluent Software. The CFD simulation of the DCMD module included smooth and rough surfaces at the bottom of the hot fluid channel to observe the heat transfer coefficients. The rough surface channels in the simulation were created using cubic blocks with a checkerboard arrangement based on each roughness level. Initially, the simulation was conducted with a smooth surface channel under identical operating conditions as the reported experiment, followed by repetitions with different surface roughness channels for fair comparison. The simulation results were then compared to the reported experimental data to validate the CFD model. The relationships between the heat transfer coefficient, Nusselt number, and mass flux to the channel surface roughness of MD modules were identified during the simulation. The results revealed that higher channel surface roughness levels corresponded to higher Nusselt numbers, higher hot fluid heat transfer coefficients, higher mass flux, and better performance of the DMCD module. The authors also conducted simulations with different flow configurations and operating conditions to validate and verify the trend of the

effect of using different surface roughness channels on DCMD performance. Overall, the simulation results were reliable as the simulation results closely predicted the mass flux compared to the reported experimental results.

Bahar, Hawlader and Ariff (2015) investigated the effect of using channelled coolant plates compared to traditional flat plates affects the performance of MD desalination in freshwater production. A small experiment utilising specially made channelled and flat plates in the MD module was carried out to measure the heat and mass transfer. For a fair and accurate comparison, the experiment was first performed using a flat plate and then repeated using a channelled plate with fins under the same experimental conditions. In both cases, different coolant side temperatures were applied, and the feed side temperature varied during the experiment, but the flow rate and fluid utilised on the feed side and coolant side were kept constant. For both experiments, the relationship between temperature, distillate flow, and plate design in the MD module was observed and evaluated. The results of the experiments demonstrated that the introduction of the "fin effect" to the MD module improved the performance of membrane distillation by increasing the distillate flux and production rate for the finned plate in comparison with the traditional flat plate. This was attributed to the increased heat transfer coefficient and mass flux that enhanced the condensation rate. Furthermore, both finned and flat plate experiments showed that higher coolant and feed temperatures led to higher mass flux and production. In order to verify the distillate flux from the experimental results, the authors proceeded on to develop a one-dimensional (1D) heat transfer model utilising channelled plates with three different types of fin designs: square, round, and triangular. The simulation showed that heat transfer was influenced by the perimeter of the fins, with a greater perimeter resulting in a higher distillate flux. This was demonstrated in the simulation, where heat transferred by square fins was slightly higher than round fins, while round fins transferred heat more efficiently than triangular fins due to their larger surface area and perimeter in contact. Finally, the developed model was considered reliable as the simulated results closely matched the experimental data.

The study conducted by Ho, et al. (2013) investigated the effect of roughened-surface flow channels on flux enhancement in DCMD desalination by using both experimental study and theoretical analysis. The idea was to

determine the optimal roughness level, considering the trade-off between enhancing mass flux and increasing energy consumption due to increased friction loss resulted by the rough surface. The authors fabricated the roughened-surface channels using siphonic-blasting with aluminium oxide sand grains, followed by coating with Nickel film using an arc spraying method. Initially, experiments were conducted with a smooth surface channel, varying hot fluid temperatures and flow rates. The relationship between the relative surface roughness and the heat transfer coefficient was subsequently evaluated by repeating the experiments with three different levels of roughness. To provide a fair comparison with the experimental results, a theoretical model was developed for simulation under identical conditions to the experiment. The results from the experiment revealed that, for the smooth surface, increasing fluid flow rate and hot fluid temperature led to an increase in mass flux due to higher heat transfer coefficient and vapor pressure. For all three roughened surfaces, similar effects were observed with respect to varying hot fluid temperature and fluid flow rate. Nonetheless, the experimental results showed that higher surface roughness levels led to increased mass flux and heat transfer coefficients, albeit with a concurrent rise in friction loss. Lastly, theoretical model simulations were carried out to verify the experimental results and to investigate temperature profiles and mass flux enhancement inside the DCMD modules in order to determine the optimal roughness level.

2.5 Effect of Spacer on DCMD Performance

Ve, et al. (2019) investigated the performance of a DCMD module with and without spacers through a heat transfer analysis experiment. The authors conducted experiments using both spacer-filled and empty channels under identical operating conditions. The spacers used in the study were made of plastic and stainless-steel materials. Various fluid flow rates were employed to validate and verify the impact of spacers on DCMD performance, with constant feed and permeate fluid temperatures maintained throughout the experiment. A counter-current flow configuration was utilized. The relationship between the heat transfer coefficient and the heat rate in relation to the presence of spacers was identified. The results showed that the heat transfer coefficient in both plastic and stainless-steel spacer-filled channels was significantly higher than in

empty channels, with the plastic spacer exhibiting a slightly higher coefficient than the stainless-steel spacer. This difference was attributed to the larger diameter of the filaments in the plastic spacer, resulting in larger wake and higher convective heat transfer. Additionally, the heat rate was considerably higher in spacer-filled channels compared to empty channels, leading to higher predicted freshwater production in the former. Overall, the experimental results demonstrated that DCMD systems using spacers exhibited better performance compared to systems without spacers.

The research conducted by Taamneh and Bataineh (2017) investigated on the methods to enhance the performance of a DCMD module by utilizing spacer-filled channels. The authors conducted both CFD simulations and experimental analyses to examine the effects of spacer presence and filament orientation on heat transfer enhancement within the DCMD module. Using the Gambit mesh generator software, the authors developed and generated a 3D CFD model of the DCMD module and grid. Initially, the simulation was conducted with an empty spacer channel under specific operating conditions. The simulation results were then compared with experimental data obtained under the same conditions and configuration to validate the CFD model. Subsequently, simulations were performed with spacers featuring different filament orientations but under identical operating conditions. The simulation identified the relationship between the Nusselt number and heat transfer coefficient concerning spacer presence and filament orientation. The results from the simulation indicated that the Nusselt number in spacer-filled channels consistently showed higher values compared to empty spacer channels, with an increase observed in channels with higher top filament angles. Similarly, the simulation results showed that the heat transfer coefficient in spacer-filled channels was consistently higher than empty spacer channels, with higher coefficients observed in channels with higher top filament angles. This increase was attributed to the generation of wakes induced by presence of spacers, with channels featuring higher top filament angles generating greater wakes and turbulence, thereby increasing the heat transfer coefficient. Consequently, the Nusselt number increased with the heat transfer coefficient, resulting in overall enhanced performance of the DCMD module with spacer-filled channels.

Overall, the simulation results exhibited good agreement with experimental data, indicating the reliability of the simulations.

Chang, et al. (2015) explored the influence of spacer-filled channels on heat transfer efficiency in DCMD systems through CFD simulations. The authors utilized the Fluent Software to conduct 3D simulations focusing on fluid flow friction, heat transfer, and mass transfer within the DMCD modules. The 3D CFD models were constructed by the authors based on the experimental modules for the simulations. The simulation results were subsequently compared to the experimental data obtained from the experiment using the L8T90 and L11T45 modules for model validation. Initially, the authors simulated empty channels under the same operating conditions as the reported experimental setup and then replicated the simulations with spacer-filled channels of different hydrodynamic angles and mesh sizes for comparison. The simulations identified relationships between mass flux and heat flux regarding the type of channels used in the DCMD module. Results from the simulations showed that average mass flux and heat flux were higher in modules with spacer-filled channels compared to modules with empty channels. This was attributed to heat and mass fluxes decreasing along the empty channel module while maintaining higher levels in the spacer-filled channels module, but with a fluctuating pattern caused by the repetitive structure of the spacer. Moreover, the simulation results revealed that local heat and mass fluxes in modules with spacer-filled channels having higher hydrodynamic angles and smaller mesh sizes were slightly lower than modules with spacer-filled channels having smaller hydrodynamic angles and larger mesh sizes. However, averaged heat and mass fluxes in modules with spacer-filled channels having higher hydrodynamic angles and smaller mesh sizes were higher than modules with smaller hydrodynamic angles and larger mesh sizes. Overall, the simulation results closely matched the experimental data, indicating the reliability of the CFD model for simulations.

The study conducted by Chang, et al. (2017) investigated the internal transfer characteristics of DCMD systems using channels with and without spacers through CFD simulation. The authors utilized Fluent 6.3 and a grid generation preprocessor GAMBIT to conduct 3D CFD simulations to understand how spacers influence DCMD system performance. Computational

models were developed based on three experimental modules: the empty channel module, L8T90, and L11T45 modules. The L8T90 module featured spacer-filled channels with a mesh size of 8 mm and a hydrodynamic angle of 90 degrees, while the L11T45 module had spacer-filled channels with a mesh size of 11 mm and a hydrodynamic angle of 45 degrees. Initially, simulations were conducted with empty channels, the L8T90 module, and the L11T45 module under the same operating conditions as the reported experimental setup. The accuracy of the computational models was validated by comparing the simulation results to the reported experimental data. Subsequently, simulations were run using a range of hot fluid inlet temperatures to verify the impact of spacers on DCMD performance. Throughout the simulations, the hot and cold fluid flow rates remained constant. The simulations identified relationships between mass flux, heat transfer coefficient, and Nusselt number concerning the presence of spacers in the DCMD system. The simulation results showed that mass flux was significantly higher in spacer-filled channels than in empty channels, with slightly higher mass flux observed in the L8T90 module compared to the L11T45 module. Additionally, the average heat transfer coefficient in spacer-filled channels was considerably higher than in empty channels, attributed to fluctuating heat transfer coefficients along spacer-filled channels. Moreover, the Nusselt number was higher in spacer-filled channels compared to empty spacer channels. However, for the L11T45 module under the same power consumption, the Nusselt number was higher than for the L8T90 module due to a slightly higher friction factor in the L8T90 module, resulting in increased eddy promoters and power consumption. Therefore, the performance of the DCMD system with the L11T45 module was better than DCMD system with the L8T90 module when considering the trade-off between power consumption and heat and mass transfer enhancement.

In the study conducted by Swaidan, et al. (2024), the performance of DCMD modules using triply periodic minimal surfaces (TPMS)-based spacers through CFD simulations is investigated. The authors developed a 3D CFD model using Star-CCM+ software to analyse the thermal and mass flux performance in a DCMD module with spacers. Validation of the 3D CFD model was achieved by comparing the simulation results to the reported experimental data. CFD simulations were conducted with Fischer-Koch S TPMS spacer,

commercial Net-type spacer, and an empty channel under identical operating conditions for a fair and accurate comparison. The relationships between hydraulic and thermal performance and the presence of spacers were identified during the simulations. The simulation results revealed that the Fischer-Koch S spacer exhibited the highest mass flux, followed by the commercial spacer and then the empty channel. This was attributed to the Fischer-Koch S spacer not only demonstrated the most uniform mass flux distribution along the channel length but also induced greater turbulence, resulting in a reduction of the boundary layer near the membrane surface and consequently enhancing the flux. Moreover, the thickness of the thermal boundary layer was observed to be smaller in the spacer-filled channel compared to the empty channel. Furthermore, the thermal performance was best with the Fischer-Koch S spacer, as evaluated by the temperature polarisation coefficient and the Nusselt number, which were highest in the Fischer-Koch S spacer. Despite the improvement in DCMD module performance with the use of spacers, there was a higher pressure drop, leading to increased power consumption. However, overall performance was determined by using a normalized power ratio, considering the trade-off between power consumption and hydraulic and thermal improvements. Consequently, the DCMD module with the Fischer-Koch S spacer outperformed both the commercial spacer and the empty channel in terms of overall performance.

Yadav, et al. (2022) investigated the performance of DCMD modules with spacer presence through CFD simulations. The authors developed a 2D CFD model based on the DCMD module to simulate and analyse the performance parameters of DCMD modules with and without spacers in both the feed and permeate channels. The 2D CFD model was developed based on several assumptions, such as simulating under steady-state conditions, assuming laminar flow, neglecting heat loss to the atmosphere, and considering only vapor molecules transported from the feed channel to the permeate channel. Simulations of the CFD model were conducted with and without spacers under identical operating conditions for an accurate comparison. The relationship between performance parameters, such as mass flux, temperature polarization coefficient, and heat transfer coefficient, which correlated with the presence of spacers, was identified in the simulations. The simulation results showed that

the mass flux was higher in the DCMD module with spacer-filled channels than in empty channels. This was because the introduction of spacers in the channels reduced boundary layer resistance, resulting in increased flow mixing and mass transfer. Additionally, the temperature polarization coefficient and the heat transfer coefficient were higher in the presence of spacers, leading to higher thermal efficiency. The authors later conducted simulations using spacers with different distances between two successive spacer filaments. The simulation results showed that both mass flux and temperature polarization coefficient increased when the distance between two successive spacer filaments increased. However, thermal efficiency remained nearly constant even when the distance between two successive spacer filaments increased because thermal efficiency mainly depended on membrane characteristics and feed temperature. Therefore, the distance between two successive spacer filaments had an insignificant effect on thermal efficiency. Overall, the simulation results indicated that the DCMD module with spacer presence had much better performance than the DCMD module without spacers.

In the study conducted by Kim, et al. (2018), the effect of different spacers on DCMD performance was investigated through experimental study and theoretical analysis. A theoretical model was developed by the authors based on the experimental module to analyse the influence of spacers adjacent to the membrane on permeate flux enhancement in the DCMD module. The theoretical analysis was conducted under the same operating conditions as the experiment, and the theoretical results were subsequently compared with the experimental data for model validation. Initially, the experiment was carried out with empty channels under specific operating conditions. Subsequently, the experiment was repeated with different spacers applied to the feed channel, permeate channel, or both sides of the feed and permeate channels under the same operating conditions. The relationship between permeate flux and the presence of different spacers was identified in the experiment. The experimental results consistently showed that the mean permeate flux in the DCMD module with spacers was always higher than in empty channels. The experimental results indicated that the highest mean permeate flux occurred when spacers were present in both the permeate and feed channels, followed by their presence solely in the feed channel and then solely in the permeate channel. Additionally,

the experimental results showed that reducing the overall thickness of the spacer and increasing the hydrodynamic angle led to an increase in both permeate flux and heat transfer coefficient. Therefore, the maximum flux enhancement and the best performance were achieved with the DCMD module using the thinnest and densest spacer with a hydrodynamic angle of 90 degrees, adjacent to both surfaces of the composite membrane. Overall, the experimental results closely matched the theoretical results, indicating the reliability of the theoretical model.

Ni, et al. (2022) investigated the enhancement of heat and mass transfer in DCMD modules with different spacer structures through CFD simulations. A 3D CFD model was developed by the authors based on the reported experimental module to conduct the simulations. The authors initially ran simulations with both empty channels and channels filled with straight spacers under the same operating conditions as the reported experiment. The simulation results were subsequently compared with the reported experimental data for model validation purposes. The authors then replicated the simulations with channels filled with novel curved spacers under the same operating conditions to ensure accurate comparison. The simulations identified the relationship between the heat transfer coefficient, permeate flux, temperature polarization coefficient, and mixing performance, all of which correlated with the spacer structures. The simulation results indicated that the DCMD module with curved spacer-filled channels exhibited a higher heat transfer coefficient compared to module with straight spacer-filled channels due to the higher Nusselt number. This resulted in better heat transfer performance in modules with curved spacer-filled channels. Moreover, the simulations showed that module with curved spacer-filled channels had a higher permeate flux compared to module with straight spacer-filled channels. Additionally, the turbulence effect caused by the curved spacer was greater than the straight spacer, leading to a higher temperature polarization coefficient and better mixing performance in modules with curved spacer-filled channels. However, the use of curved spacers also resulted in a higher pressure drop compared to straight spacers, leading to increased energy consumption. Despite this disadvantage, the simulation results indicated that modules with curved spacer-filled channels still exhibited the best overall performance when considering the trade-off between power consumption and heat and mass transfer enhancement. Overall, the simulation

results closely matched with the experimental data, indicating the reliability of the 3D CFD model for simulations.

2.6 Effect of Multiple Channels Module on DCMD Performance

The study conducted by Ali et al. (2024) investigated the effect of using a multiple channels module on improving the water production rate in a DCMD system. The new multiple channels DCMD module introduced by the authors in this study consisted of three channels in total, with the permeate channel in the middle and two feed channels, one on each side, separated by the membrane. The authors first ran the DCMD experiment with the conventional DCMD module, which had one feed channel, and one permeate channel, under different experimental conditions, varying inlet velocities and inlet feed temperatures. The authors then repeated the experiment with the newly introduced multiple channels DCMD module under identical experimental conditions as the conventional DCMD module for a fair and accurate comparison. The relationship between the types of DCMD modules used and the flux and productivity of the DCMD system was monitored and analysed during the experiment. The experimental results showed that the flux and productivity of the DCMD system with the multiple channels module were always 100% higher than those of the DCMD system with the conventional module under all conditions. This indicated that the newly introduced multiple channels design improved the water production rate and performance of the DCMD system. The authors later conducted further experiments with the multiple channels module, but with varying feed channel thicknesses, to investigate how different channel designs affected DCMD productivity and efficiency under identical experimental conditions. The results showed that when the thickness of the feed channels decreased, the productivity and efficiency of the DCMD system increased. This was due to the shorter diffusion path in the thinner feed channel, allowing water vapor molecules to cross the membrane more easily, leading to higher productivity. However, the results also showed that excessive reduction in channel thickness led to pressure drops across the channel, increasing energy consumption for pumping. The authors then conducted CFD simulations with the multiple channels module under the same operating conditions for further

validation and verification. Overall, the experimental results were reliable as the experimental results closely matched the simulation results.

2.7 Summary

This section explains that the performance of the DCMD process can be improved by several methods discussed in various studies. One method to enhance the performance of the DCMD system is to use a counter-current flow configuration rather than a co-current flow configuration, as studies have shown that the former can lead to higher permeation flux and a greater temperature driving force. Some studies indicate that using a lower channel height improves performance by enhancing the heat transfer coefficient and vapor pressure difference. Another method suggested by the studies is using a rough surface channel rather than a smooth surface channel to improve mass flux and heat transfer coefficients in the system. Additionally, the use of spacer-filled channels instead of empty channels has been proposed for better heat and mass transfer performance. Finally, the use of a multiple channels module has been shown to perform better than the conventional module. Overall, the methods employed in past studies provide valuable insights and suggestions on channel designs to enhance the performance of the DCMD system, which is relevant to the focus of this study.

CHAPTER 3

METHODOLOGY AND WORK PLAN

3.1 Introduction

In this chapter, the methodology and work plan for the project will be outlined and elaborated upon. Section 3.2 will illustrate the research flow with a flowchart, and Section 3.3 will describe the experimental setup. Following that, Section 3.4 will explain the experimental procedure for this study, while Section 3.5 will detail the experimental and design parameters. Section 3.6 will present the parameters to be tested in the experiment. Additionally, Section 3.7 will provide drawings of the flat block and finned blocks with different designs, and Section 3.8 will explain the block fabrication process. Section 3.9 will present the project planning using a Gantt chart. Finally, Section 3.10 will summarize the chapter.

3.2 Flowchart

The flowchart of the overall process for this study is illustrated in Figure 3.1. The flowchart outlines the process from the start to the end of the study. The study began with understanding the project topic, followed by conducting journal research on the topic and filtering out unwanted journals. Next, project planning was carried out to ensure that everything was workable and could be completed within the given timeframe for the final year project. Subsequently, the finned blocks were fabricated according to the planned method. The experiment was then conducted based on the planned method and procedures. If the experiment for a block type failed, it was rerun until successful results were obtained. The results from the experiment with each block type were then analyzed. Finally, report writing was initiated and completed within the given period.

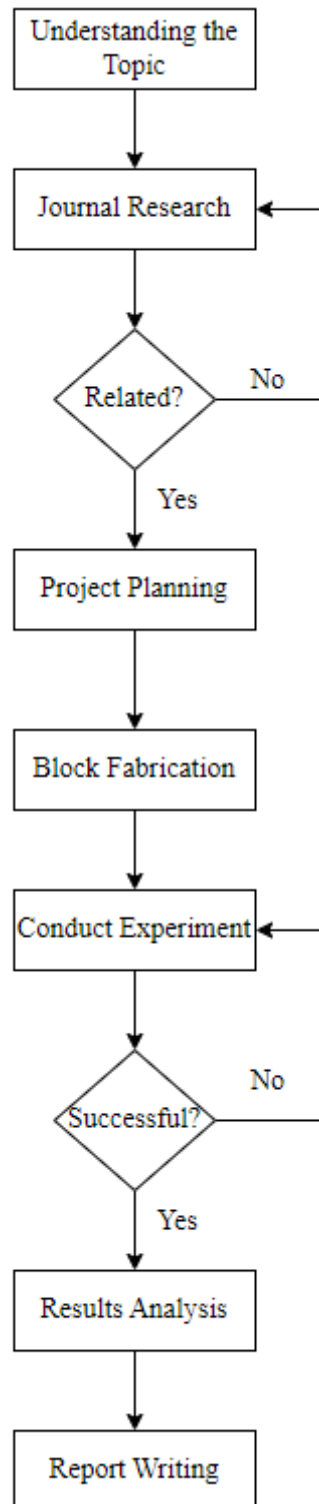


Figure 3.1: Flowchart of the overall process.

3.3 Experimental Setup

Figure 3.2 illustrates the schematic diagram of the experimental setup for the DCMD experiment in this study, while Figure 3.3 shows the actual experimental setup for the DCMD experiments. The apparatus used includes a feed tank, a permeate tank, and a DCMD module. Additionally, the required equipment and materials consist of a hydrophobic membrane, silicon tubing and piping, gasket, block, weighing scale, heater, peristaltic pump, and thermocouples.

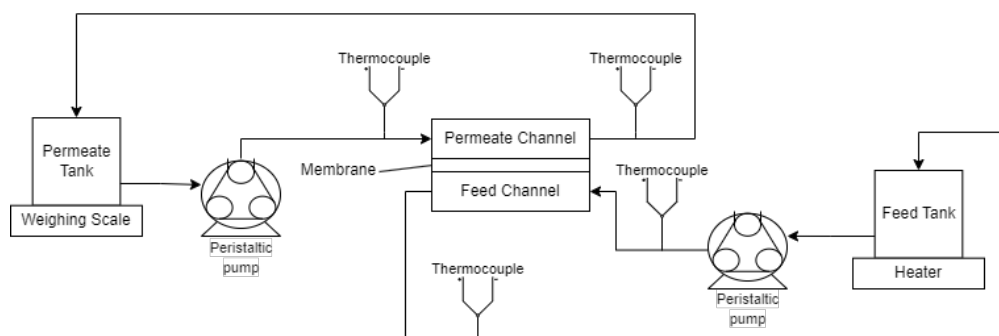


Figure 3.2: Schematic Diagram of the DCMD experimental setup.

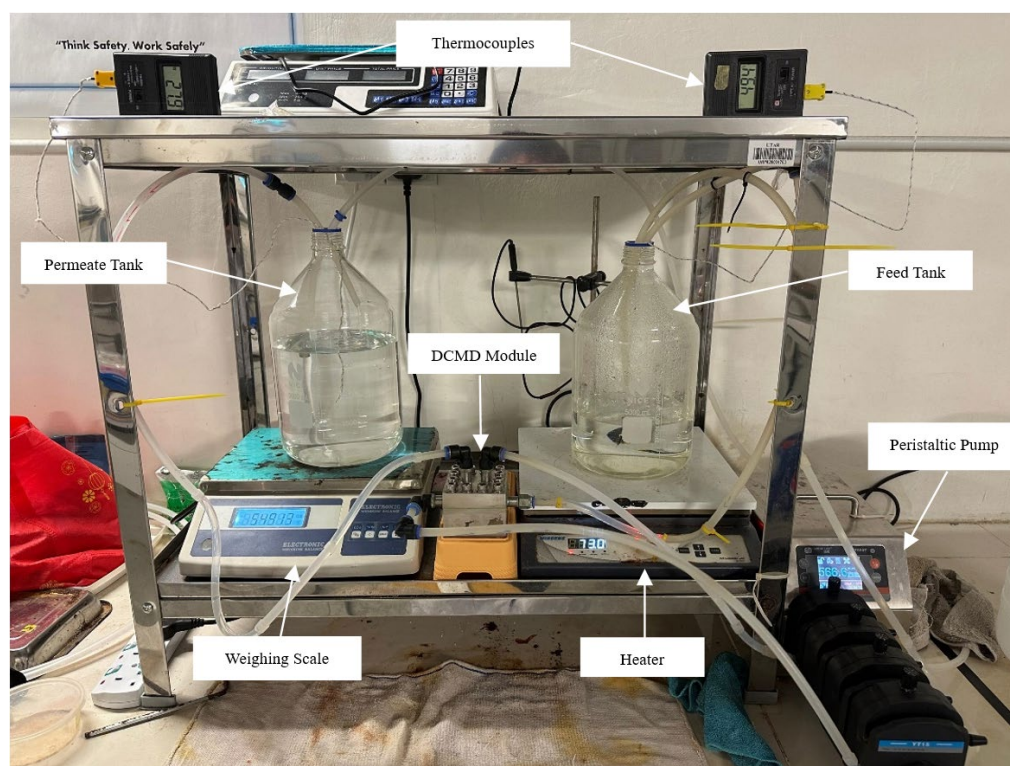


Figure 3.3: Actual DCMD experimental setup.

3.4 Experimental Procedure

To begin the DCMD experiment, both the permeate and feed 4.5-liter tanks were first cleaned and rinsed with distilled water to ensure there were no impurities that could affect the solution concentration later. Subsequently, the permeate tank was filled with distilled water up to 4 liters to prepare the permeate solution and placed on the weighing scale, which was then reset to zero before starting the experiment. The conductivity of the distilled water in the permeate tank was measured in PPM using a conductivity meter. Next, the feed tank was filled with 2 liters of distilled water, and 70 grams of salt was weighed (using the ratio of 35 grams of salt per liter) and added to the feed tank to prepare a 3.5 wt.% NaCl saline solution to synthesize seawater (Ho, et al., 2014). The mixture was stirred thoroughly to ensure uniform dissolution of the salt, resulting in the desired concentration of the solution. The heater was then activated, and the feed tank was placed on it. Throughout the experiment, the heater remained operational and was adjusted periodically to maintain the target temperature of 50°C for the feed solution. The module assembly involved correctly arranging the feed channel, block, gasket, support, membrane, support, gasket, and permeate channel in sequence. Then, 12 nuts were used to securely tighten the module. To initiate the experiment, the peristaltic pump was activated and adjusted to 200 rpm, with the flow rate recorded at 566.6 ml/min. Subsequently, the temperature and weight of the permeate solution, as well as the temperature of the feed solution, were recorded at 10-minute intervals until the experiment ended at 130 minutes. Finally, the permeate was tested again with a conductivity meter to ensure it complied with Malaysia's drinking water standards.

The correct assembly sequence of the DCMD module is shown in Figure 3.4, while Figure 3.5 illustrates the permeate conductivity measurement using a conductivity meter.

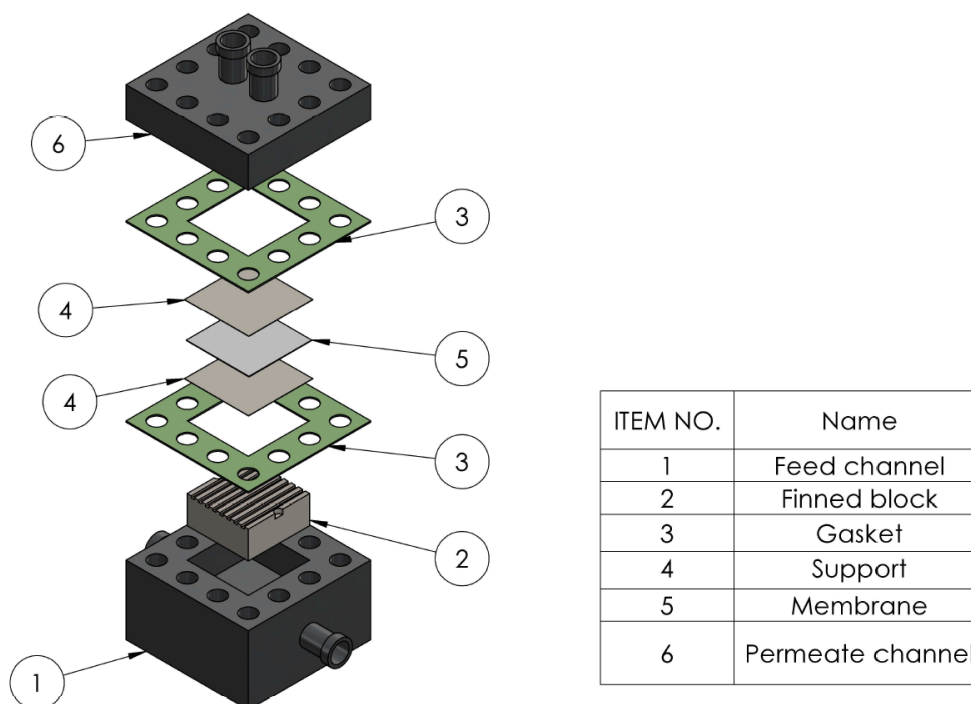


Figure 3.4: Assembly of DCMD module.



Figure 3.5: Permeate conductivity measurement using conductivity meter.

3.5 Parameters for the Proposed Study

The experiment for this study was conducted at UTAR Sungai Long, KB 514. The proposed experimental parameters are listed in Table 3.1, and the design parameters are listed in Table 3.2.

Table 3.1: Experimental parameters for the proposed study

Experimental Parameter	Value
Quantity of Permeate Solution	4 litres
Quantity of Feed Solution	2 litres
Concentration of Feed Solution	3.5 wt.% NaCl
Salinity of Feed Solution	35000 PPM
Conductivity of Feed Solution	55000 $\mu\text{S}/\text{cm}$
Target feed temperature	50°C
Peristaltic Pump speed	200 rpm
Permeate and Feed Flow rate	566.6 ml/min
Flow Configuration	Counter-current flow

Table 3.2: Design parameters for the proposed study

Design Parameter	Value
Dimensions of Block	40 mm x 40 mm x 18 mm
Channel Height-to-Width Ratio	0.62
Channel Height, H	0 mm to 2.46 mm
Fin-to-channel Width ratio, W_f / W ratio	0 to 3.56
Number of Fins	7 to 9

In the channel design of the finned block in this study, the channel height and fin height were the same and referred to the same parameter. The locations of the parameters, channel height (H), channel width (W), and fin width (W_f), are illustrated in Figure 3.6.

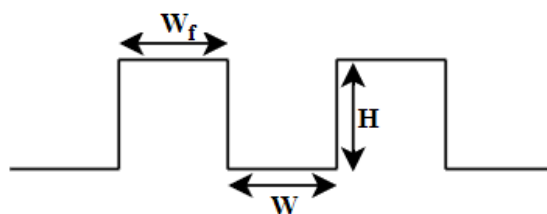


Figure 3.6: Locations of parameters H , W , and W_f in the channel design.

3.6 Parameters Tested in the Experiment

In this study, various parameters were tested to observe their effects on the performance of the DCMD system. However, the primary aim was to investigate how different channel designs affected the performance of the DCMD system by determining the water production rate, specifically through measuring the average permeate flux and comparing it to that of a conventional DCMD module. The channel designs were modified by using finned blocks with varying designs. The parameters studied included channel height, fin-to-channel width ratio, and the number of fins. Additionally, other parameters, such as the temperature difference between the permeate and feed, which affected the temperature gradient, were tested to assess their impact on the permeate flux in DCMD systems with different finned blocks.

3.7 Design of Finned Blocks

This section presents 9 drawings of a flat block and 8 finned blocks with different channel designs, which were used in the experiment, as shown in Figures 3.7 to 3.15. Table 3.3 summarizes the specifications for all the block designs.

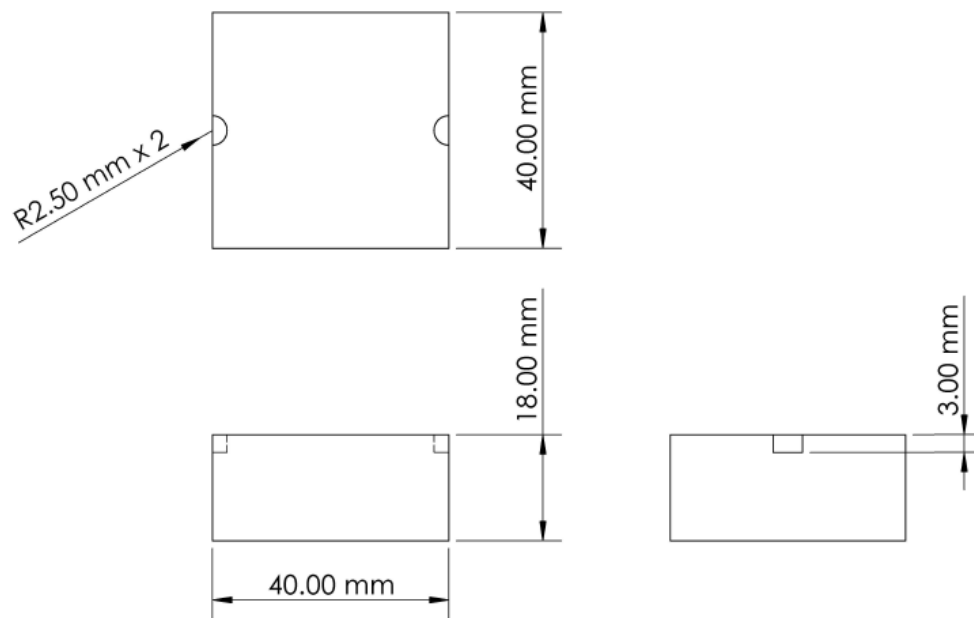


Figure 3.7: Drawing of the flat block design.

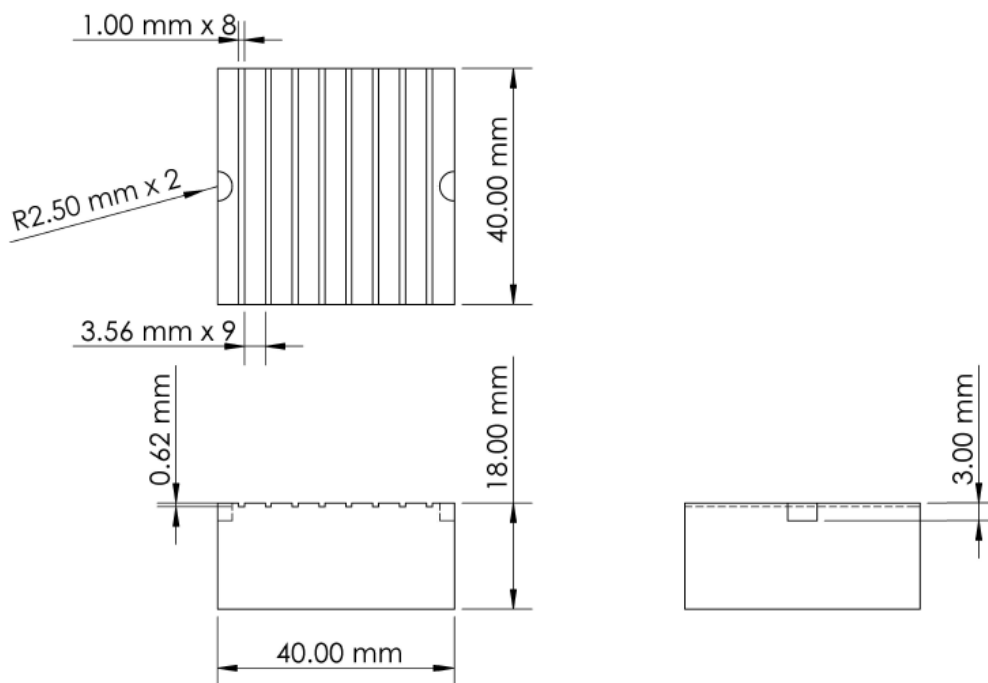


Figure 3.8: Drawing of the Type 1 finned block design.

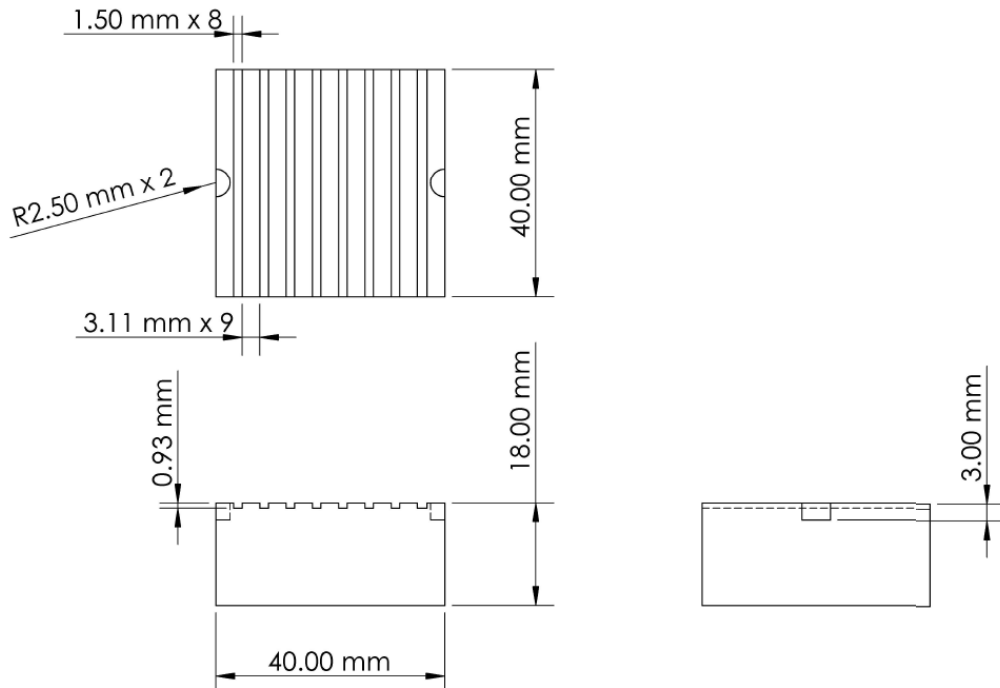


Figure 3.9: Drawing of the Type 2 finned block design.

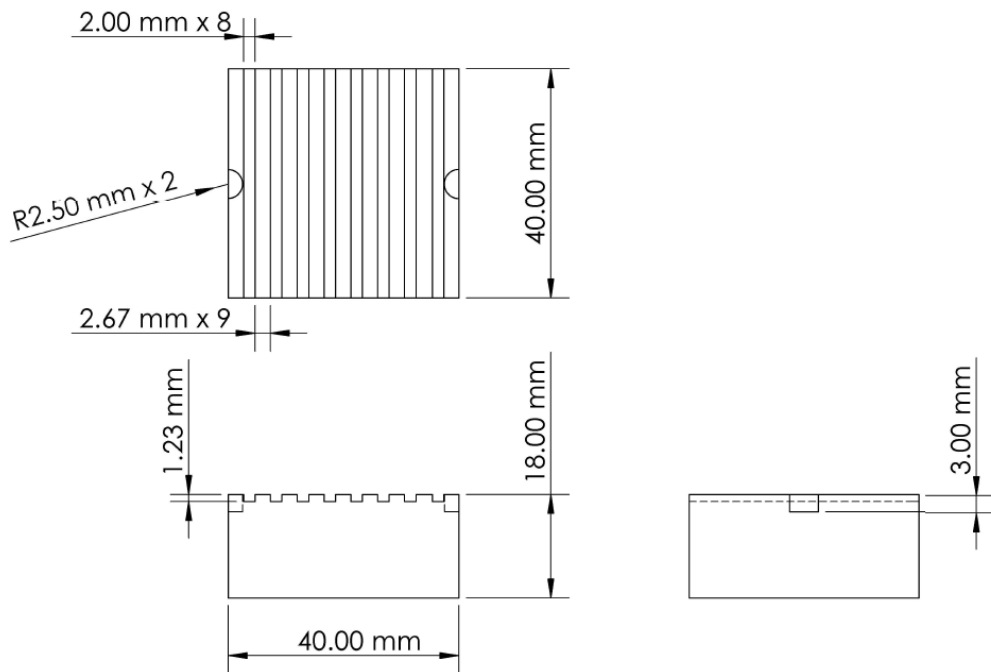


Figure 3.10: Drawing of the Type 3 finned block design.

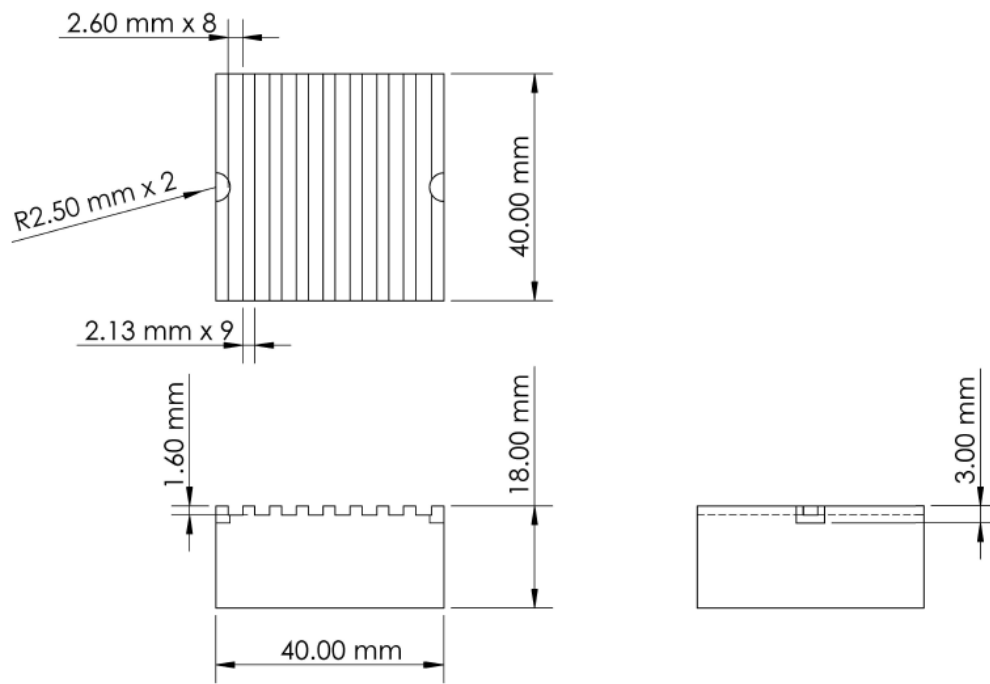


Figure 3.11: Drawing of the Type 4 finned block design.

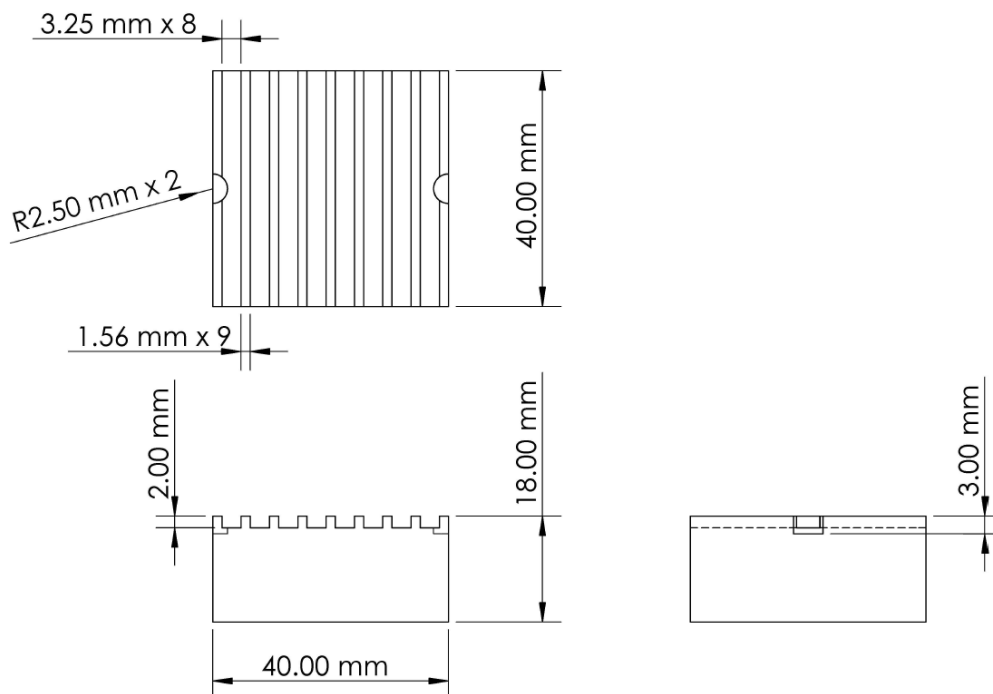


Figure 3.12: Drawing of the Type 5 finned block design.

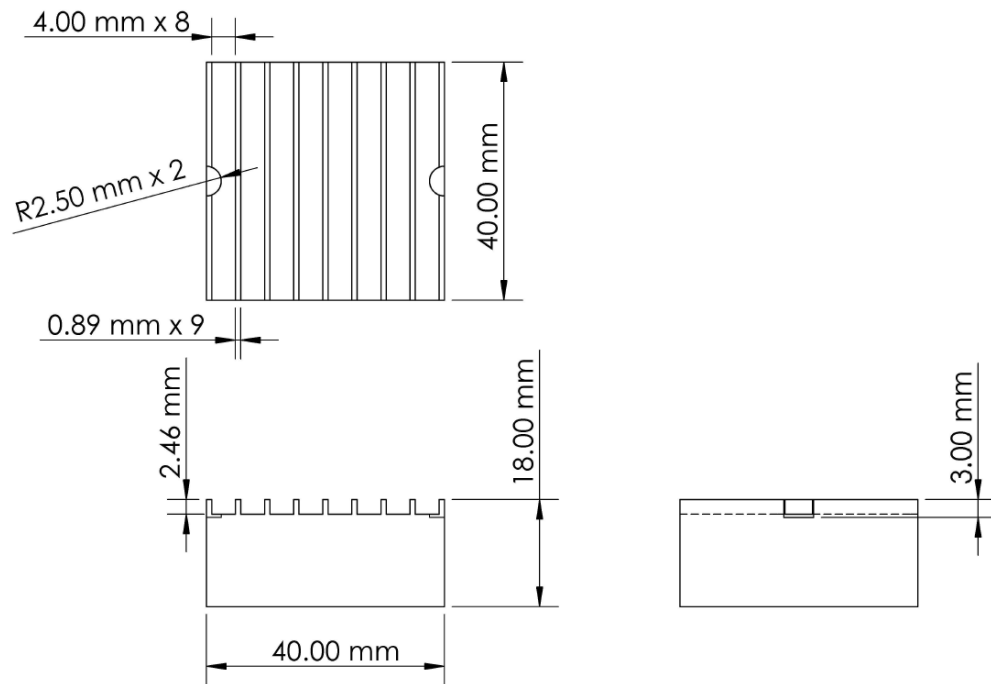


Figure 3.13: Drawing of the Type 6 finned block design.

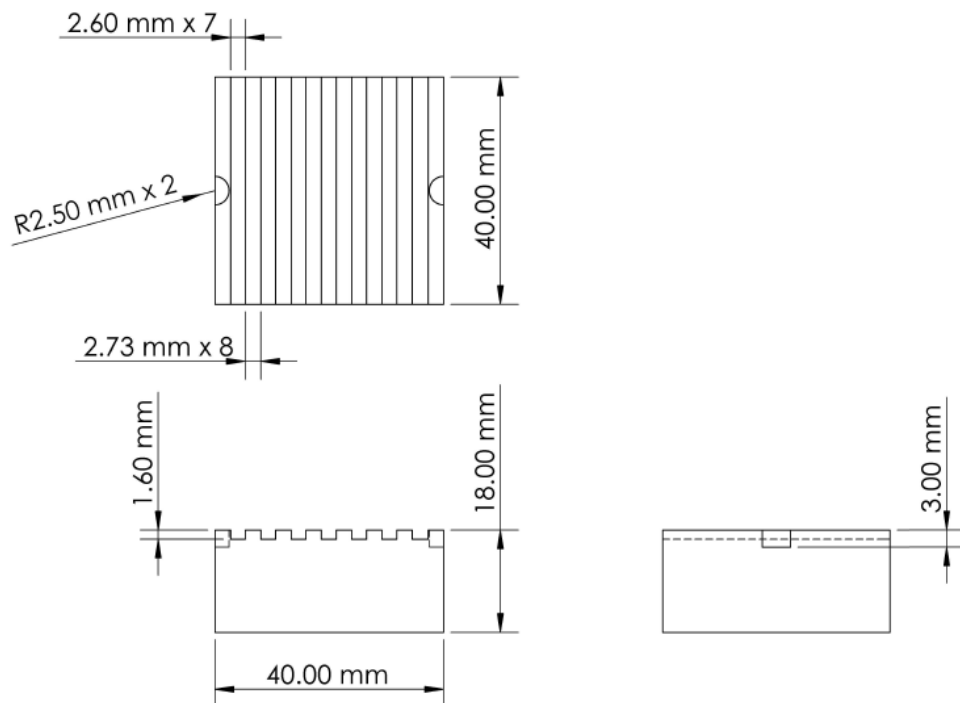


Figure 3.14: Drawing of the 8-fin finned block design.

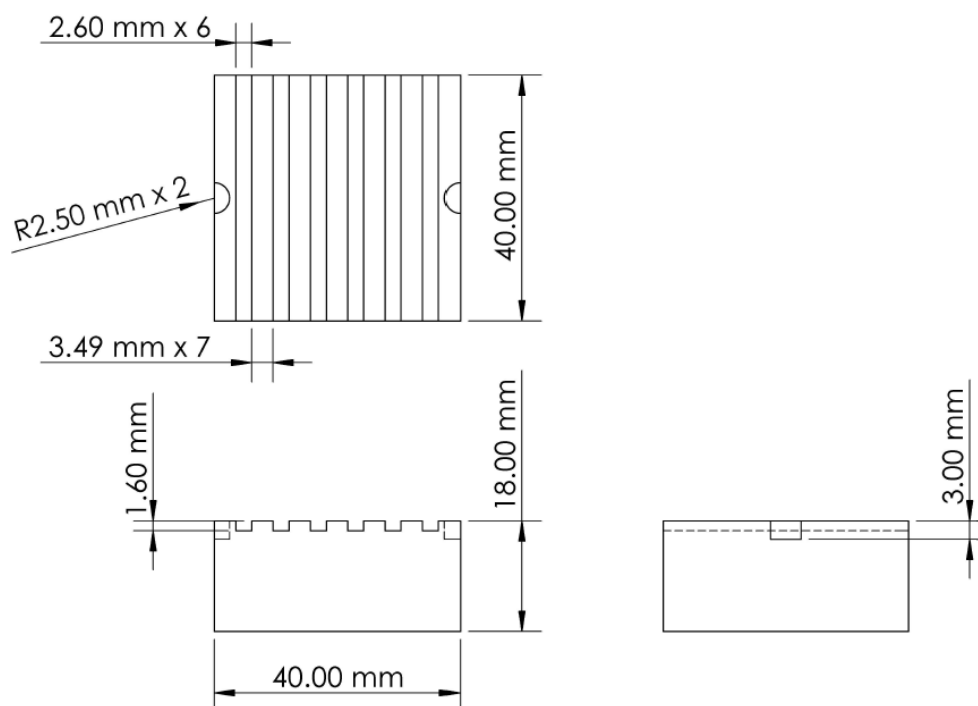


Figure 3.15: Drawing of the 7-fin finned block design.

Table 3.3: Specifications for all block designs.

Type	No. of Fins	Channel Height, H (mm)	Channel Width, W (mm)	Fin Width, W_f (mm)	W_f/W ratio
Flat	0	0	0	0	0
1	9	0.62	1	3.56	3.56
2	9	0.93	1.5	3.11	2.07
3	9	1.23	2	2.67	1.34
4	9	1.60	2.6	2.13	0.82
5	9	2.00	3.25	1.56	0.48
6	9	2.46	4	0.86	0.22
8-fin	8	1.60	2.6	2.73	-
7-fin	7	1.60	2.6	3.49	-

3.8 Fabrication Process for Finned Blocks

The fabrication of blocks began with drawing the 3D models and designs in SolidWorks based on the design parameters to be studied. Next, the drawings were printed and brought to the UTAR workshop. The suitable raw material for

the experiment, which was aluminum, was selected. This was because DCMD was a water-based system, so the material chosen had to be able to resist rust corrosion when in contact with the saline water in the feed channel. Additionally, aluminum was easy to machine, cut, and shape into complex designs, which had the properties required for this experiment. Since the channel design was in millimeters, the tools used had to be very thin in diameter. If the material were too hard, it might lead to tool breakage during channel fabrication. Furthermore, aluminum was relatively more affordable compared to other metals with the required properties, especially considering that multiple finned blocks needed to be fabricated (ASM International, 2023). After that, the aluminum was cut into several small blocks using the band saw cutter in the workshop, and these blocks were later milled to precise dimensions of 40 mm x 40 mm x 18 mm using the milling machine. G-codes were then written based on the printed drawings of the channel designs for each block. Next, a suitable milling cutter was selected for each channel design, and the blocks with dimensions of 40 mm x 40 mm x 18 mm were set up at the CNC milling machine. After CNC milling, the finned blocks with different channel designs were finally fabricated.

Figure 3.16 illustrates the raw material used for the blocks. The cutting process of the aluminum with a band saw cutter is depicted in Figure 3.17. Figure 3.18 details the milling process for the aluminum blocks. The preparation of G-code for CNC milling is shown in Figure 3.19. Figure 3.20 demonstrates the CNC milling of channels on the blocks, and Figure 3.21 presents the finned block samples created following the block fabrication process.



Figure 3.16: Aluminum as raw material for block fabrication.



Figure 3.17: Cutting aluminum using a band saw cutter.



Figure 3.18: Milling of aluminum block to desired dimensions using a milling machine.

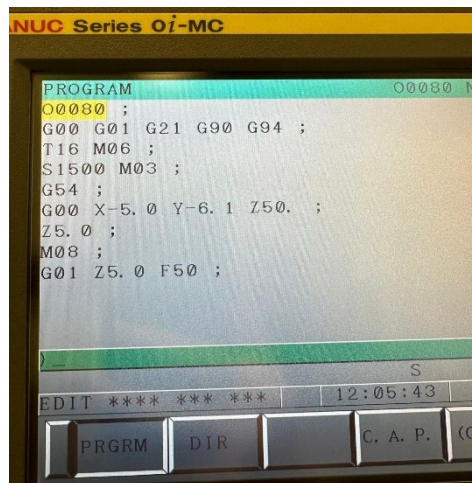


Figure 3.19: Inserting G-code into the CNC control panel.



Figure 3.20: CNC milling of channels on the block.

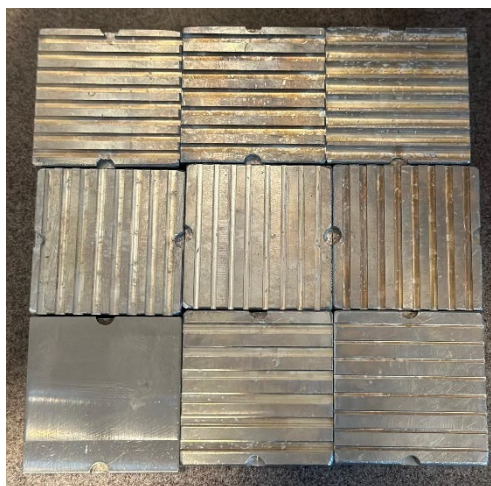


Figure 3.21: Fabricated finned block samples.

3.9 Gantt chart

In the FYP 1 Gantt chart, the period from week 2 to week 4 was the stage of understanding and getting familiar with the project title, conducting research, and looking for journals relevant to the FYP topics. Week 5 to week 8 represented the stage of filtering unwanted journals, only retaining those discussing methods like the FYP objectives. With enough materials on hand, literature review writing could commence. This stage was allotted a 4-week period due to the scarcity of relevant journals, requiring additional time. Week 8 to week 10 was the stage of finalizing the literature review, followed by planning, and writing the report introduction. Week 10 to week 12 involved finalizing the introduction, then planning and writing the methodology and workplan. Week 12 to week 13 was the stage of finalizing the FYP report and conducting a thorough check of the entire document. Finally, week 14 was for submitting the FYP 1 report and preparing slides and materials for presentation. The FYP 1 Gantt chart is illustrated in Figure 3.22.

No.	Project Activities	W1	W2	W3	W4	W5	W6	W7	W8	W9	W10	W11	W12	W13	W14
1	Project comprehension, planning, and research.		■	■	■										
2	Begin literature review after assessing journal content.					■	■	■	■						
3	Continue literature review writing and draft introduction.								■	■	■				
4	Finalize introduction, plan, and write methodology and work plan.										■	■	■		
5	Finalize and review FYP 1 report, covering chapters 1 through 3.												■	■	
6	Submission of FYP 1 report and presentation.														■

Figure 3.22: Gantt chart for FYP 1.

In the FYP 2 Gantt chart, week 1 was the stage of preparing the lab materials to be used in the DCMD experiment. Weeks 2 to 3 were dedicated to fabricating blocks with different designs to create channels with varied configurations. Weeks 3 to 7 were spent conducting the DCMD experiment and recording the results. This stage was allotted 5 weeks because each DCMD experiment took nearly 3 hours to finish. Since not every experiment was successful and failures occurred, the 5-week period ensured that all experiments could be completed successfully. Next, weeks 7 to 8 were devoted to analyzing the results and determining and validating trends. Weeks 8 to 10 involved

writing the report discussion and creating graphs to illustrate the study's trends. Weeks 10 to 12 focused on writing the report conclusions and suggesting recommendations for the experiment. Weeks 12 to 13 entailed checking the report, finalizing it, and compiling it if there were no changes or errors. Lastly, week 14 was designated for FYP 2 report submission and presentation. The FYP 2 Gantt chart is illustrated in Figure 3.23.

No.	Project Activities	W1	W2	W3	W4	W5	W6	W7	W8	W9	W10	W11	W12	W13	W14
1	Lab material preparation.	■													
2	Fabricaiton of blocks with different designs.		■	■											
3	Conduct experiments and record results.			■	■	■	■	■							
4	Result analysis.							■	■						
5	Chapter 4: Results and Discussion report writing.								■	■	■				
6	Chapter 5: Conclusion and Recommendations report writing.										■	■	■		
7	FYP 2 report compilation.												■	■	
8	FYP 2 report submission and presentation.														■

Figure 3.23: Gantt chart for FYP 2.

3.10 Summary

In this chapter, the procedure for conducting the experiment and the method for fabricating the blocks to be tested were outlined in detail. The experimental parameters were fixed, while the design parameters were determined for the study. The block designs, which featured different channel configurations, were clearly depicted in the drawings based on these design parameters. Varying design parameters, such as channel height, fin-to-channel width ratio, and the number of fins, resulted in different channel designs for each block. These varying channel designs were used to test their effects on the performance of the DCMD system. The work plan for the study was presented with a flowchart and a Gantt chart. The results associated with each design parameter were analyzed in Chapter 4 to further understand the relationship between these parameters and the water production rates of the DCMD system.

CHAPTER 4

RESULTS AND DISCUSSION

4.1 Introduction

According to Jimenez-Hornero et al. (2008), there are three types of flow regimes based on the aspect ratio (H/W) of the height of roughness (H) to the gap between obstacles (W). The three flow regimes are isolated roughness flow, wake interference flow, and skimming flow. Isolated roughness flow occurs when H/W is less than 0.3, wake interference flow occurs when H/W is approximately 0.5, and skimming flow occurs when H/W is approximately 1. In the study by Cheong (2024), the author defined the aspect ratio, with H referring to the channel height and W to the channel width. Based on these three flow regimes, the author created channel designs with different channel height-to-width (H/W) ratios in the 9-fin block with dimensions of 40 mm x 40 mm x 18 mm to investigate the effect on DCMD performance. It was found that the channel with an H/W ratio of 0.62, corresponding to wake interference flow, gave the best performance among the blocks with other H/W ratios. This channel design, with a 0.62 ratio, had a channel height of 1 mm, a channel width of 1.625 mm, and a fin width of 3 mm, resulting in an average weight increment of 4.12 g and an average permeate flux of 4 g/(m²s). However, the H/W ratio of 0.62 can be achieved through different combinations of channel height, channel width, and fin width. Therefore, there is uncertainty regarding how changes in channel height, fin-to-channel width (W_f/W) ratio, and the number of fins, while maintaining a consistent H/W ratio of 0.62, affect DCMD performance, and hence this will be investigated in this work.

In this chapter, the term "flat block" refers to a block with a flat surface design or without channels, used to represent the conventional DCMD module. By fixing the H/W ratio at 0.62 and the number of fins at 9, and by varying the channel height and fin-to-channel width ratio, the first section aims to identify the critical relationship between the temperature difference and the water production rate of the DCMD module with different channel designs compared to the conventional flat design. Based on this relationship and a comparison of

the results in the first section, the second section explores the critical relationship between channel height and fin-to-channel width ratio in relation to the improvement in water production rate. Through these two sections, the channel height, channel width, and fin width close to the optimum for achieving the best DCMD performance are determined. The third section then investigates the critical relationship between the number of fins and the water production rate using the identified channel height and channel width near the optimum levels. Finally, the fourth section presents the conductivity test results for each type of block before and after the experiment.

4.2 Relationship between temperature differences and water production rates for a DCMD module with various channel designs.

Based on previous research, most studies provided experimental results on the effect of feed temperature on the water production rate in conventional DCMD modules. These studies typically kept the permeate temperature constant while varying the feed temperature to determine the impact of the temperature difference on permeate flux. Therefore, this study takes a different approach by keeping the feed temperature constant while allowing the permeate temperature to increase throughout the experiment. The temperature difference is recorded every 10 minutes, and the trend in permeate flux is investigated. Initially, the experiment begins with the conventional DCMD module as a reference. It then proceeds with DCMD modules featuring different channel designs and maintains a constant H/W ratio of 0.62 to further study and validate the influence of temperature difference on permeate flux across various designs.

Table 4.1 lists the types of blocks used to study the effect of the temperature difference between the feed and permeate on the permeate flux for a DCMD module with different channel designs in this section.

Table 4.1: Types of blocks used.

Blocks Used
Flat Block
Type 1 Block
Type 2 Block
Type 3 Block
Type 4 Block
Type 5 Block
Type 6 Block

The raw experimental data for the flat block and blocks of types 1 through 6 are presented in Tables A-1 to A-7 in Appendix A, with the permeate flux calculated based on the weight increase recorded during the experiment. This data is then used to analyze the relationship between the temperature difference between the feed and permeate on the permeate flux for the DCMD module with each channel design, as summarized in Figure 4.1. Figure 4.2 summarizes the changes in permeate flux over time during the experiment.

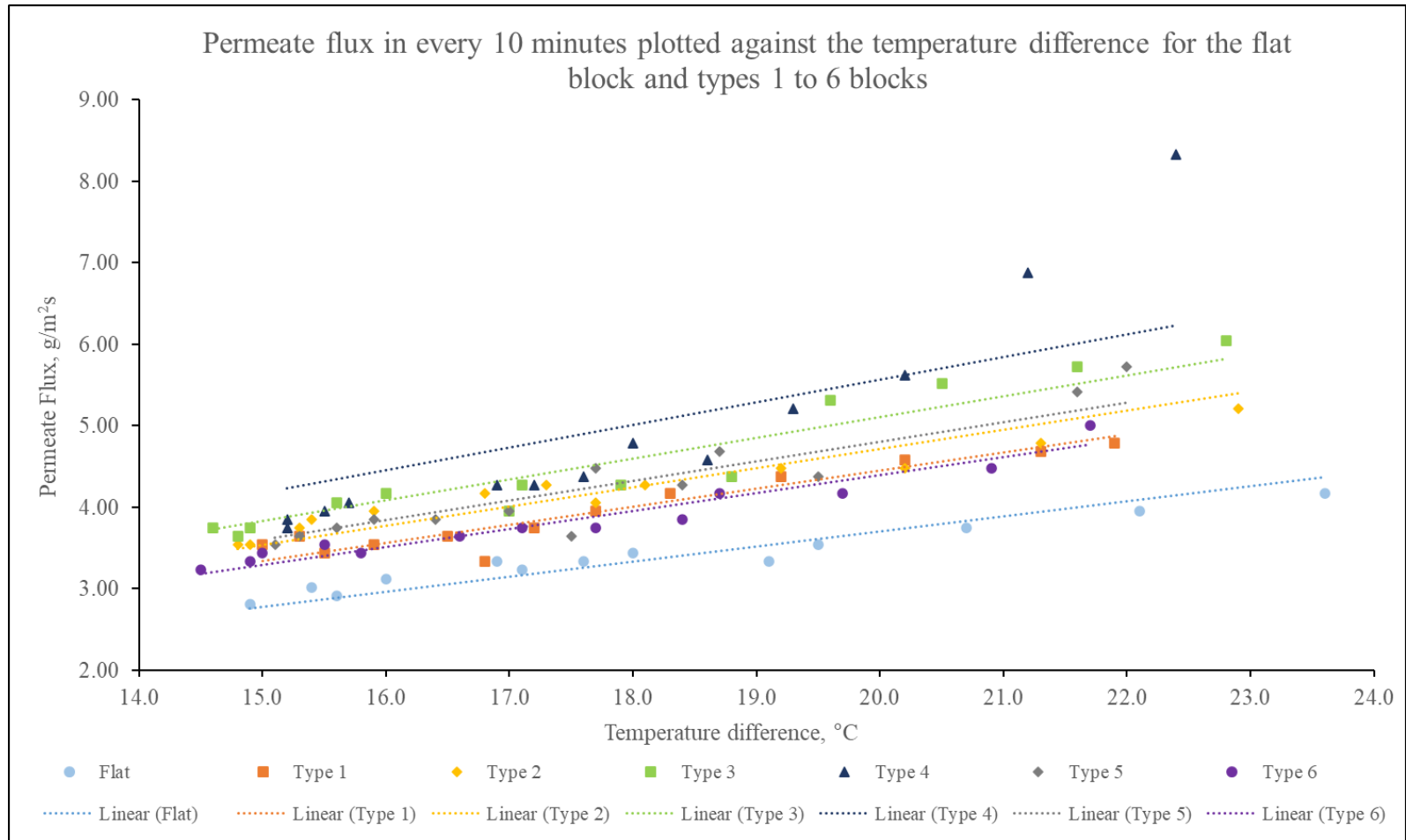


Figure 4.1: Permeate flux in every 10 minutes plotted against the temperature difference for the flat block and types 1 to 6 blocks.

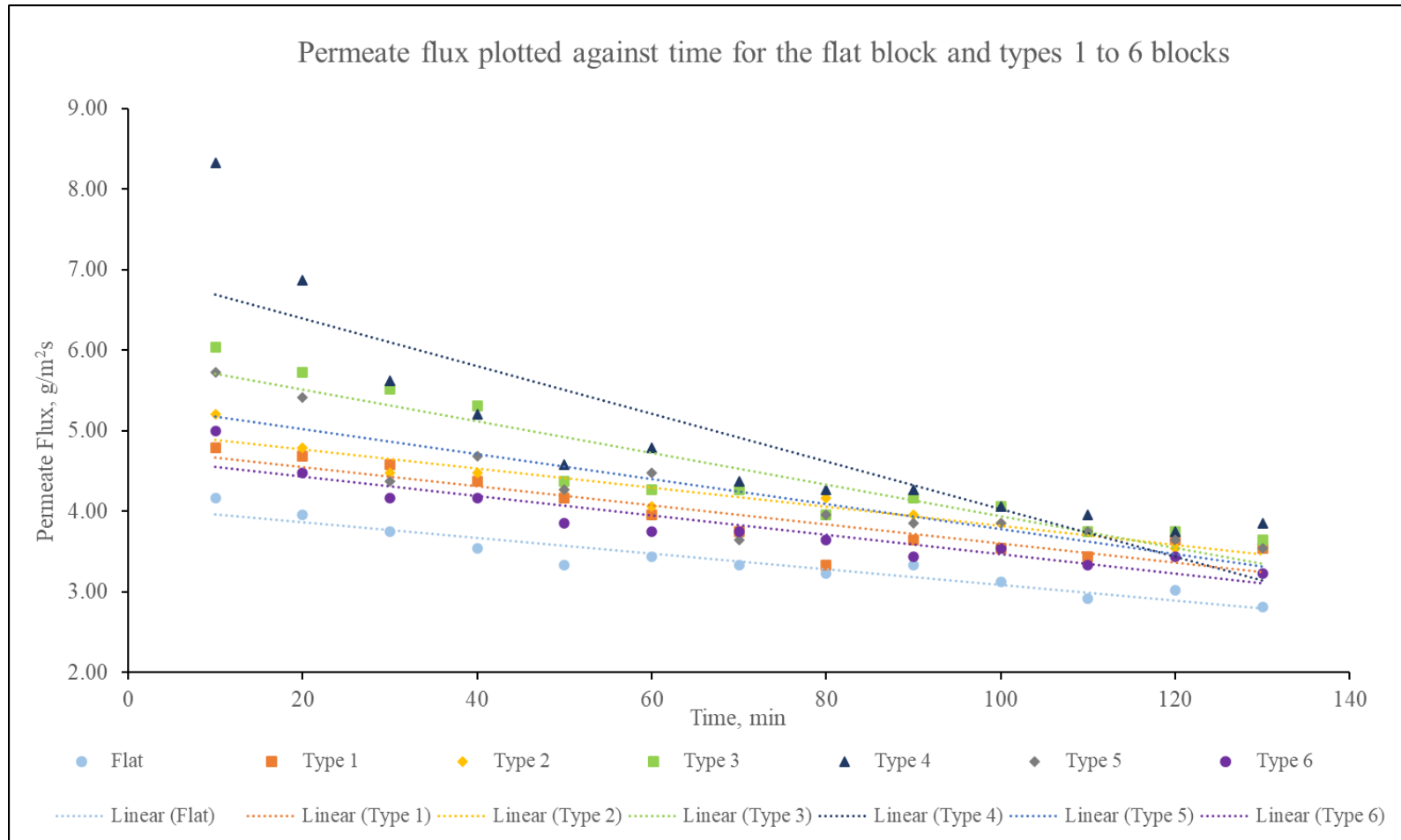


Figure 4.2: Permeate flux plotted against time for the flat block and types 1 to 6 blocks.

Based on the graphs in Figures 4.1 and 4.2, similar clear overall trends can be observed across the different types of blocks. At the beginning of the experiment, the permeate flux measured every 10 minutes are usually the highest throughout the entire experiment. As time progresses, the permeate flux start to decrease. This occurs because, at the start of the experiment, the permeate temperature is the lowest before coming into contact with the feed solution. As a result, the largest temperature difference occurs at the beginning, leading to the highest permeate flux during the first 10 minutes. However, as time increases and the permeate solution comes into contact with the feed solution, the temperature of the permeate solution rises, reducing the temperature difference between the feed and permeate solutions. Consequently, the permeate flux decrease as the temperature difference decreases. This is because lower temperature difference leads to a lower vapor pressure difference, which reduces the effective driving force and lowers system productivity (Rabie, Elkady, and El-Shazly, 2021).

Ideally, since the temperature difference decreases as time increases, the permeate flux measured in the following 10 minutes is generally lower than the flux measured in the previous 10 minutes. However, upon closer examination, it can be observed from the experiment that a higher temperature difference may yield a lower permeate flux than a lower temperature difference, while a lower temperature difference can yield a higher permeate flux than a higher temperature difference, particularly when the temperature differences are close to each other. This could be due to several factors, one being the possibility that during this period, the rate of increase in permeate temperature slows down. As the temperatures of the two solutions approach each other, the heat transfer rate decreases due to the reduced temperature gradient. Additionally, since the feed temperature is recorded every 10 minutes and tends to fluctuate, the heater must be adjusted periodically to maintain the feed temperature close to the target of 50°C. The feed temperature during the 10-minute intervals may fluctuate higher than the temperature recorded at the end of each interval, leading to instances where a lower temperature difference results in a higher permeate flux than a higher temperature difference.

Another factor could be the common challenge faced by DCMD, which is the temperature polarization effect. The temperatures near the membrane on both the feed and permeate sides may not be the same as the bulk temperatures, which are the measured temperatures, leading to fluctuations or variations in permeate flux relative to the temperature difference. Membrane fouling could also be a contributing factor, as the experiment runs for a total of 130 minutes, a relatively long duration. Therefore, as the temperature difference decreases over time, the reduction in the effective driving force, along with the temporarily reduced effective surface area for vapor transfer, could also lead to fluctuations and variations in permeate flux. Furthermore, minor changes in heat transfer dynamics, such as small variations in turbulence and mixing effects, could lead to a non-linear relationship between temperature difference and permeate flux, especially when the temperature differences are close to each other. These small variations could cause fluctuations in permeate flux as well. Additionally, as the experiment progresses and vapor transfer continues, changes in the feed solution concentration could affect the vapor pressure on the feed side and, consequently, the permeate flux. Another factor could be slight inaccuracies in temperature and flux measurements due to the sensitivity of the instruments in handling fluctuating values, resulting in variations in permeate flux.

4.3 Relationship between channel height and the fin-to-channel width ratio in relation to the improvement in water production rate

By comparing the permeate fluxes of each block in Figures 4.1 and 4.2, it is apparent that blocks with varying channel designs produce different permeate fluxes. This suggests that both channel height and the fin-to-width ratio can significantly influence the water production rate in a DCMD module. When the average permeate fluxes obtained from the raw experimental data in Tables A-1 to A-7 in Appendix A are compiled, the trends become clearer, highlighting the effects of channel height and fin-to-width ratio on average permeate flux in the DCMD process.

Table 4.2 consolidates and compares the data from Table 3.3 and the average permeate fluxes from Tables A-1 to A-7, while Table 4.3 illustrates the

improvements in water production achieved with various channel designs compared to the conventional DCMD module.

Table 4.2: Comparison of the average permeate fluxes for different channel heights and fin-to-width ratios.

Type	Channel Height, H (mm)	W_f/W ratio	Average Permeate Flux, $g/(m^2s)$
Flat	0	0	3.17
1	0.62	3.56	3.67
2	0.93	2.07	3.94
3	1.23	1.34	4.03
4	1.60	0.82	4.21
5	2.00	0.48	3.89
6	2.46	0.22	3.55

The results from Table 4.2 are shown in Figures 4.3 and 4.4.

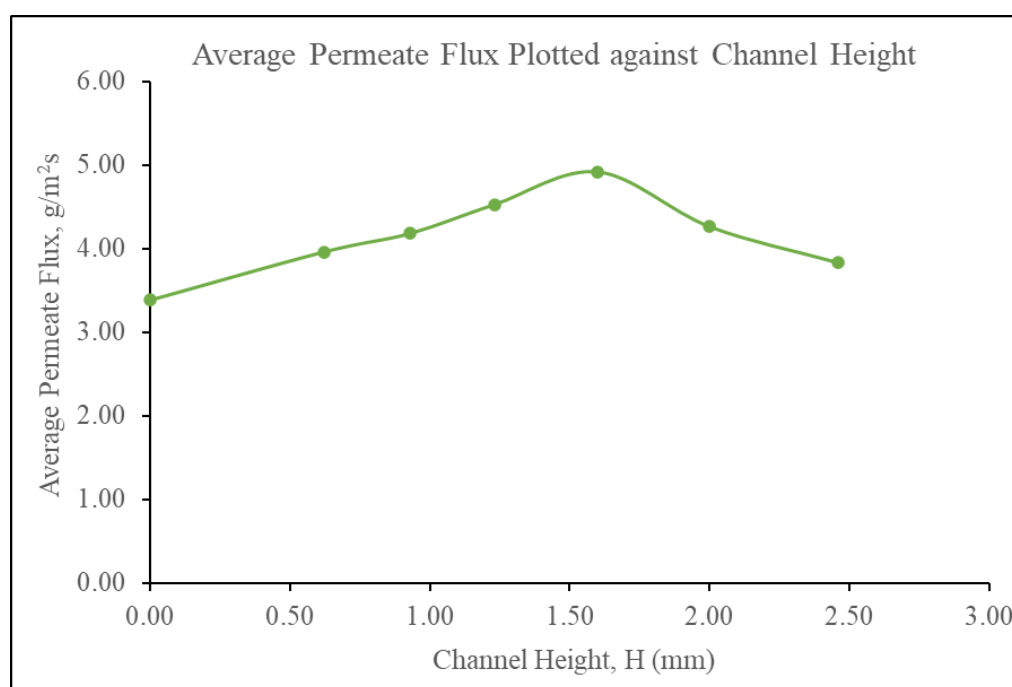


Figure 4.3: Average permeate flux for blocks with different channel heights.

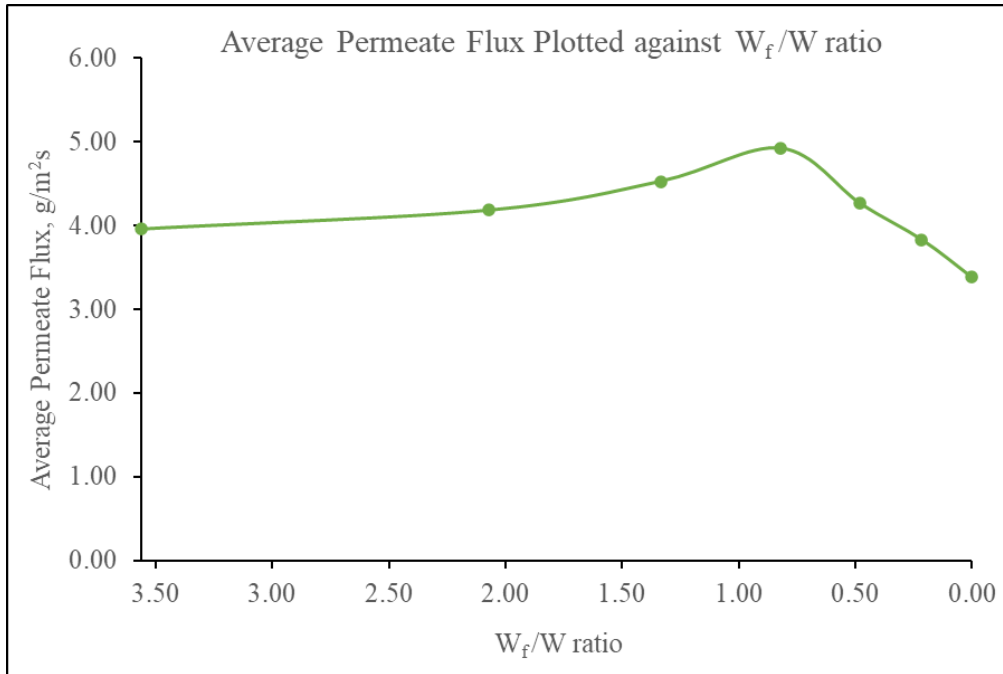


Figure 4.4: Average permeate flux for blocks with different fin-to-width ratios.

Table 4.3: Comparison of the percentage increase in average permeate flux compared to the flat block for various channel heights and fin-to-width ratios.

Type	Channel Height, H (mm)	W_f/W ratio	Percentage Increase in Flux, %
1	0.62	3.56	15.7
2	0.93	2.07	24.1
3	1.23	1.34	27.0
4	1.60	0.82	32.8
5	2.00	0.48	22.6
6	2.46	0.22	12.0

The results from Table 4.3 are shown in Figures 4.5 and 4.6.

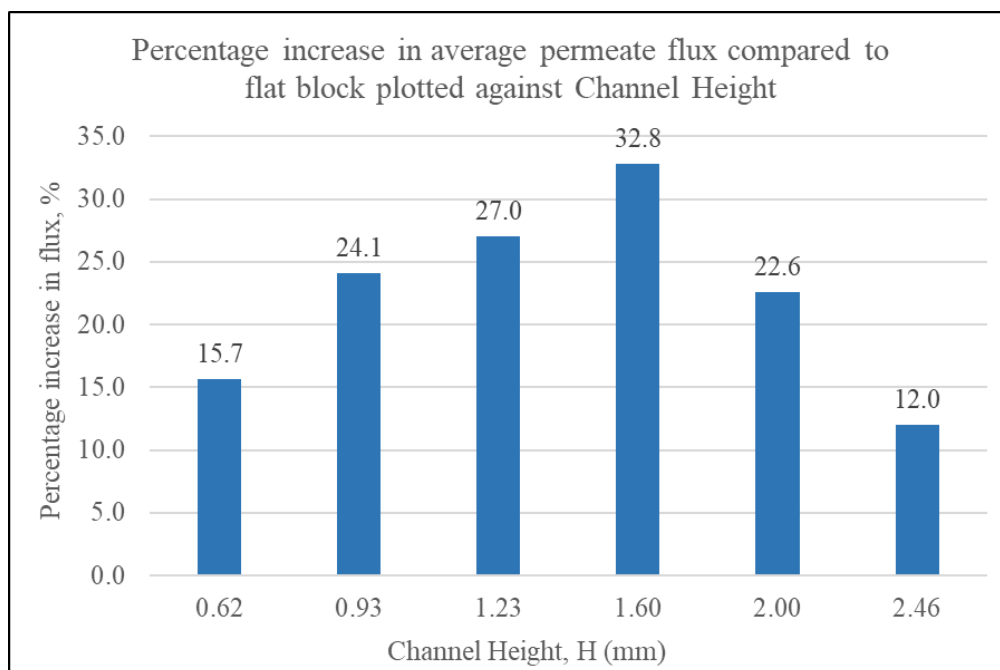


Figure 4.5: Percentage increase in average permeate flux for blocks with different channel heights.

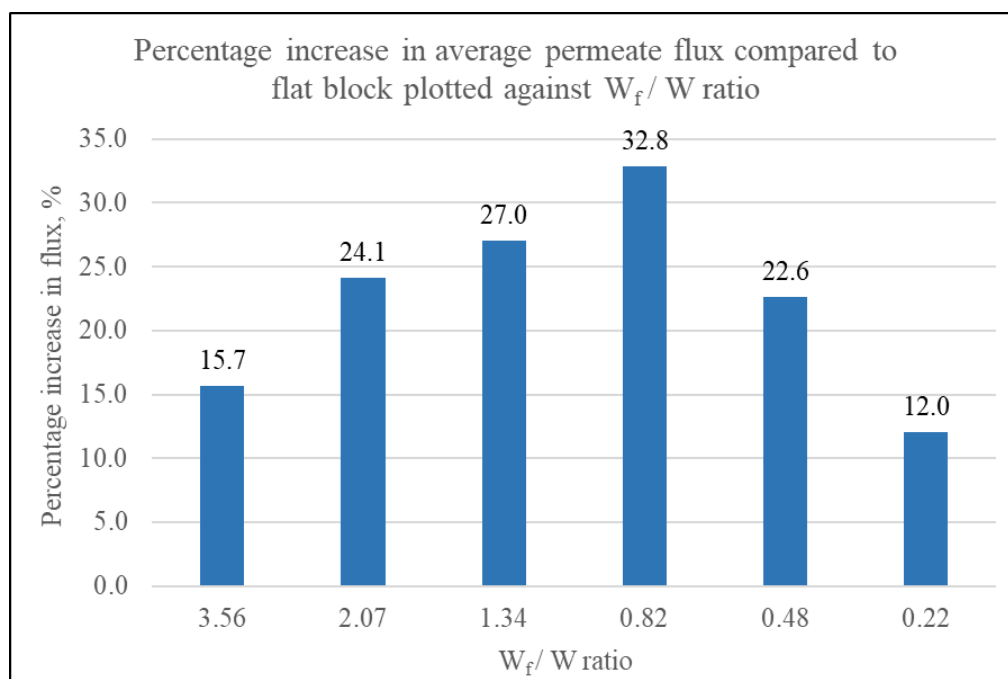


Figure 4.6: Percentage increase in average permeate flux for blocks with different fin-to-width ratios.

In a conventional DCMD module, represented by the flat block, the boundary layer is thicker, temperature distribution is uneven, and the

temperature gradient across the membrane is inconsistent. This leads to higher temperature polarization, where the effective temperature difference between the hot feed and cold permeate decreases because the temperatures on both sides of the membrane become closer to each other. Additionally, membrane fouling is more likely due to salt deposition on the membrane surface. Prolonged exposure to high temperatures can also lead to membrane degradation, which limits the allowable feed temperature and consequently reduces the temperature difference, resulting in lower permeate flux compared to a DCMD module with channels (Ahmad, et al., 2015). The DCMD module with channels introduces higher turbulence in the fluid flow, reducing the boundary layer thickness and ensuring more uniform temperature and flow distribution across the membrane. Improved turbulence enhances the mixing of the feed solution and reduces temperature and concentration polarization effects, thereby improving heat and mass transfer. Furthermore, turbulence helps to reduce membrane fouling by continuously removing salt particles from the membrane surface, resulting in higher permeate flux compared to the conventional DCMD module. However, different channel designs can produce varying levels of turbulence, resulting in different water production rates. Thus, the channel designs that are closest to the optimum need to be identified.

Based on Figure 4.3, the average permeate flux steadily increases as channel height increases until reaching an optimal level. Beyond this optimal height, further increases in channel height lead to a decrease in average permeate flux. This effect is more clearly illustrated in the improvement in water production rates shown in Figure 4.5. For instance, when the experiment was conducted with a block that had a channel height of 0.62 mm, the percentage increase in average permeate flux was 15.7%. Increasing the channel height to 1.6 mm, which is near the optimal height, resulted in the highest improvement in water production, with a 32.8% increase in average permeate flux compared to the flat block. However, as the channel height increased from 1.6 mm to 2.0 mm, the improvement in average permeate flux began to decline, decreasing from 32.8% to 22.6%. When the channel height was further increased to 2.46 mm, the improvement in water production rate dropped sharply to a 12% increase in average permeate flux, which is significantly lower than that of the

block with a channel height of 0.62 mm. The overall trend can be explained by the fact that increasing the channel height up to the optimum level increases the space available for fluid flow, enhancing turbulence and improving the mixing of the feed solution in the feed channel. This reduction in boundary layer thickness and increase in heat and mass transfer leads to a higher average permeate flux. However, when the channel height is increased beyond the optimum, the excessive height allows the fluid flow to become more laminar rather than turbulent. This occurs because the turbulent effect diminishes as the flow area in the channel increases. The greater freedom of movement reduces the disruption of the boundary layer, decreases the heat and mass transfer rates, and weakens the mixing effect in the feed solution, resulting in a decrease in average permeate flux (Zhuang, et al., 2017).

According to Figure 4.4, the average permeate flux steadily increases as the fin-to-channel width ratio decreases until it reaches an optimal ratio. Beyond this optimal ratio, further decreases in the fin-to-channel width ratio result in a sharp decline in average permeate flux. This trend is more evident in Figure 4.6, which highlights the improvements in water production rates. When the experiment was conducted with a block that had a fin-to-channel width ratio of 3.56, the percentage increase in average permeate flux was 15.7%. As the fin-to-channel width ratio decreases to 0.82, which is close to the optimal ratio, the block shows the highest improvement in water production rate in the experiment, with a 32.8% increase in average permeate flux. However, as seen in Figure 4.18, when the fin-to-channel width ratio slightly decreases from 0.82 to 0.48, the decline in water production improvement is steep. The block with a fin-to-channel width ratio of 0.48 shows only a 22.6% increase in average permeate flux, which is much lower than the blocks with fin-to-channel width ratios of 1.37 and 2.07, which show increases of 27.0% and 24.1% in average permeate flux, respectively. When the fin-to-channel width ratio further decreases to 0.22, the improvement in water production rate is the lowest among the blocks with different channel designs, with only a 12.0% increase in average flux compared to a flat block.

This overall trend can be explained by the fact that as the fin-to-channel width ratio decreases, the proportion of channel space to fin area increases. This

change results in enhanced fluid turbulence and mixing effects within the feed solution, which leads to a reduction in boundary layer thickness and increases in heat and mass transfer, ultimately resulting in a higher average permeate flux. When the fin-to-channel width ratio is close to the optimal ratio, the effects of channel width and fin surface area are balanced, creating ideal conditions for maximum turbulence and mixing within the channel and thus achieving the highest average permeate flux. However, further decreasing the fin-to-channel width ratio beyond the optimal level causes the channel width to become too large relative to the fin width. This increases the spacing between the fins, reducing the impingement and blockage effect in the feed channel. Consequently, the turbulence and mixing effect in the feed solution is reduced (Xie, et al., 2019). When the fin-to-channel width ratio approaches 0, the block becomes increasingly similar to a flat block, resulting in performance in average permeate flux that is also similar or only slightly higher than that of a flat block. Consequently, the percentage increase in average permeate flux compared to a flat block is extremely low.

Furthermore, according to the results obtained in Cheong (2024), the block with an H/W ratio of 0.62, which has the channel height of 1 mm and the fin-to-channel width ratio of 1.85, achieved an average permeate flux of 4 g/(m²s). This represents a 26.1% increase in average permeate flux compared to the flat block results obtained in this study. These results show that the block type with an H/W ratio of 0.62 studied in Cheong (2024) aligns well with the trends observed in this study, both in terms of channel height and fin-to-channel width ratio. This relationship also suggests that the performance of DCMD, in terms of water production rates, using a channel with an H/W ratio of 0.62 can be further enhanced by carefully selecting the appropriate channel height and fin-to-channel width, as there is still potential for improvement. This is further supported by the fact that the Type 3 and Type 4 blocks used in this study showed better results than the block used in Cheong (2024), with the Type 4 block being the closest to the optimum. It demonstrated the highest improvement and best performance among all the blocks studied.

4.4 Relationship between the number of fins and the water production rate

The 9-fin block with the channel design closest to the optimum is Type 4, which has a channel height of 1.60 mm, a channel width of 2.6 mm, and a fin width of 2.13 mm. By selecting this block with the best performance and maintaining its channel height and channel width constant, the blocks are further modified with different numbers of fins to compare and study the effect of the number of fins on the water production rate.

Table 4.4 lists and shows the specifications of the blocks with 9-fin, 8 fins and 7 fins selected to study the effect of the number of fins.

Table 4.4: Specifications for 9-fin, 8-fin and 7-fin blocks.

No. of Fins	Channel Height, H (mm)	Channel Width, W (mm)	Fin Width, W _f (mm)
9	1.6	2.6	2.13
8	1.6	2.6	2.73
7	1.6	2.6	3.49

The raw experimental data for the 8-fin and 7-fin blocks are presented in Tables A-8 and A-9 in Appendix A, with permeate flux calculated based on the recorded weight increase. These data are used to compare the water production rates for blocks with varying numbers of fins. The relationship between the temperature difference between the feed and permeate and the permeate flux for the DCMD module with 9-fin, 8-fin, and 7-fin blocks is summarized and shown in Figure 4.7, while Figure 4.8 summarizes the changes in permeate flux over time for the 9-fin, 8-fin, and 7-fin blocks during the experiment.

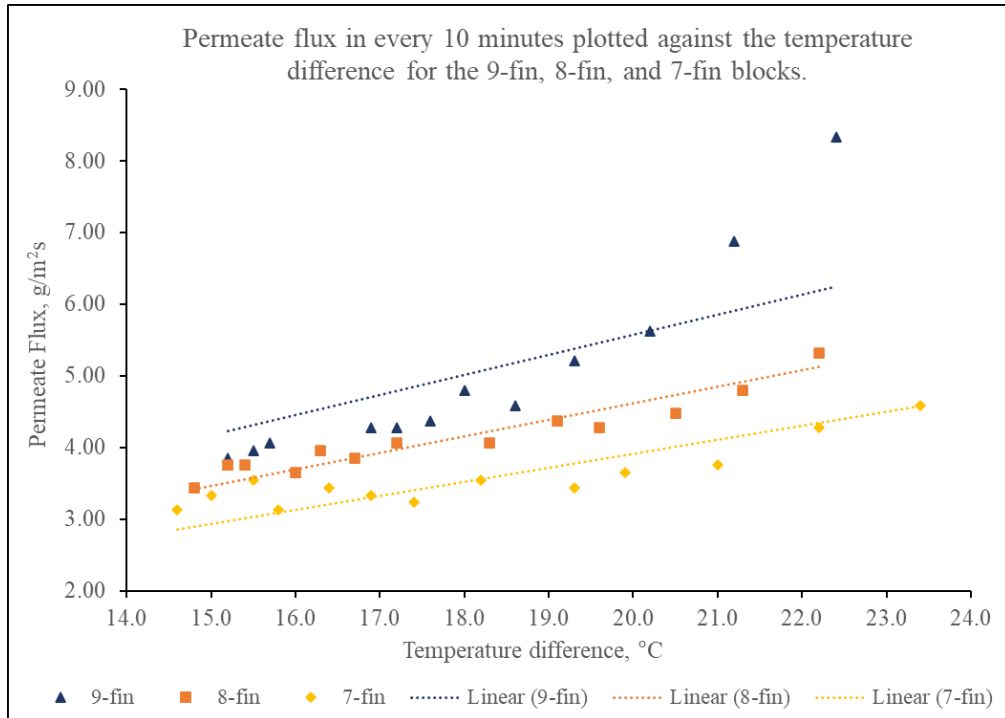


Figure 4.7: Permeate flux in every 10 minutes plotted against the temperature difference for the 9-fin, 8-fin, and 7-fin blocks.

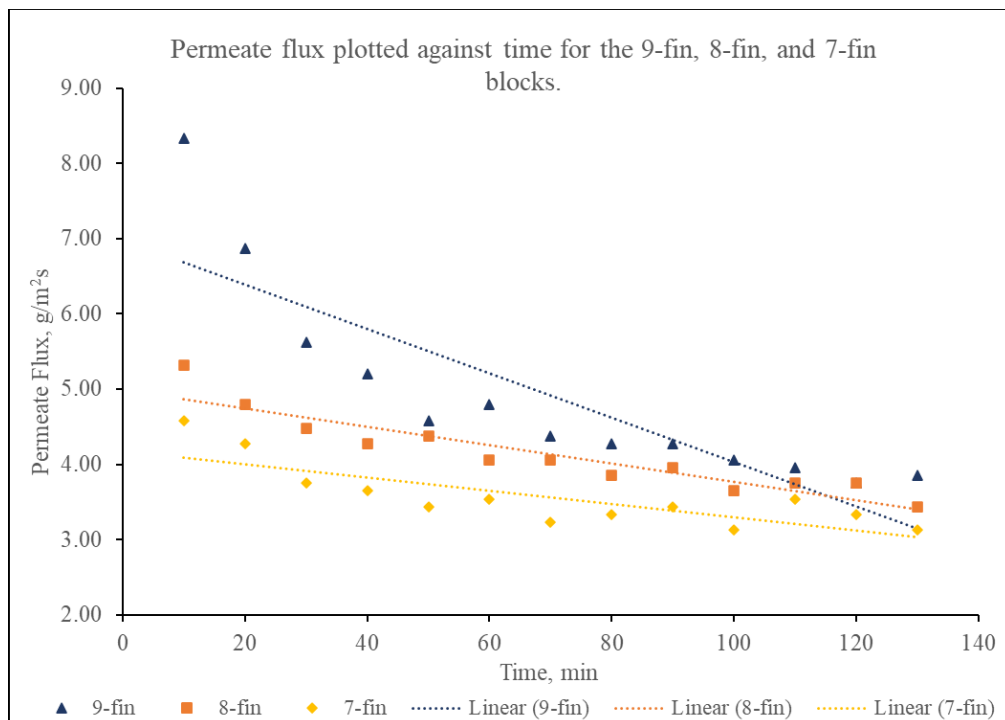


Figure 4.8: Permeate flux plotted against time for the 9-fin, 8-fin, and 7-fin blocks.

By comparing the permeate fluxes of each block in Figures 4.7 and 4.8, it is apparent that blocks with different numbers of fins produce different permeate fluxes. This suggests that the number of fins can significantly influence the water production rate in a DCMD module. When the average permeate fluxes obtained from the raw experimental data in Tables A-1 (Flat), A-5 (9 fins), A-8, and A-9 in Appendix A are compiled, the trends become clearer, highlighting the effects of fin number on average permeate flux in the DCMD process.

Table 4.5 consolidates and compares the average permeate flux based on the raw experimental data from Tables A-1, A-5, A-8, and A-9. Meanwhile, Table 4.6 illustrates the improvements in water production achieved with blocks having different numbers of fins compared to the conventional DCMD module

Table 4.5: Comparison of the average permeate fluxes for blocks with different numbers of fins.

No. of Fins	Average Permeate Flux, g/(m²s)
(Flat) 0	3.38
7	3.57
8	4.13
9	4.92

The results from Table 4.5 are shown in Figures 4.9.

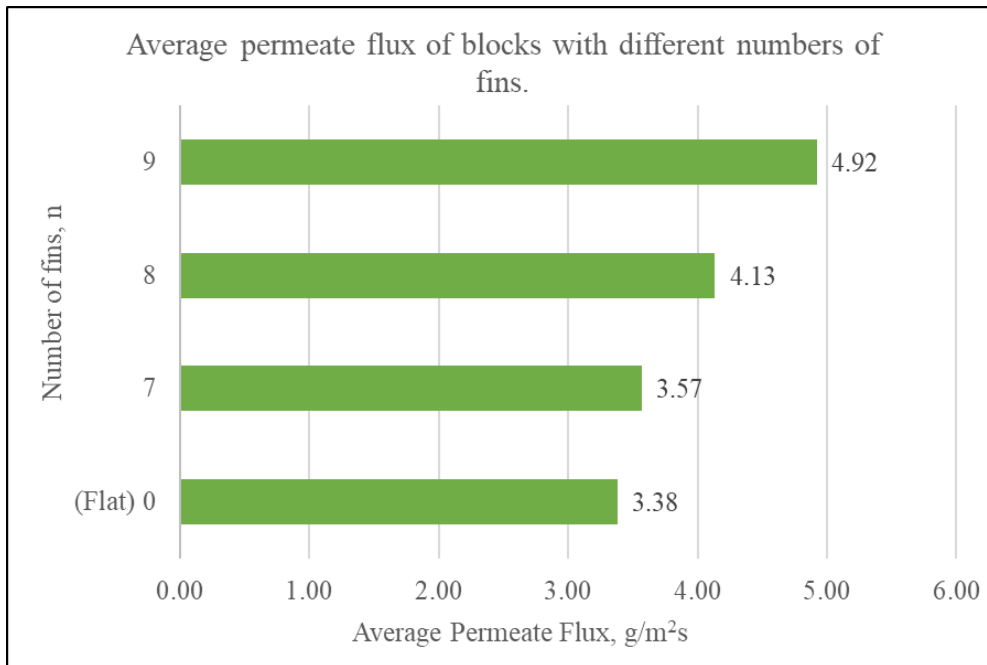


Figure 4.9: Average permeate flux of blocks with different numbers of fins.

Table 4.6: Comparison of the percentage increase in average permeate flux compared to the flat block for different numbers of fins.

No. of Fins	Percentage Increase in Flux, %
7	5.5
8	22.3
9	32.8

The results from Table 4.6 are shown in Figures 4.10.

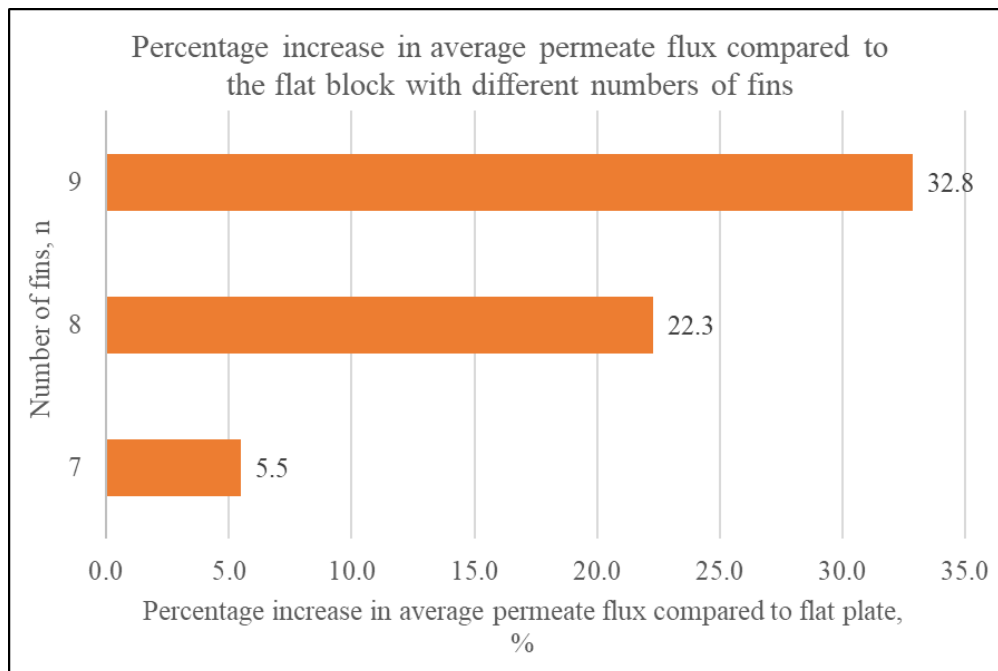


Figure 4.10: Percentage increase in average permeate flux compared to the flat block with different numbers of fins.

Based on Figure 4.9, the average permeate flux decreases as the number of fins on the block is reduced. Comparing the average permeate flux of blocks with different numbers of fins reveals that the 9-fin block has the highest average permeate flux at $4.92 \text{ g}/(\text{m}^2\text{s})$, followed by the 8-fin block at 4.13 and the 7-fin block at $3.57 \text{ g}/(\text{m}^2\text{s})$. The 0-fin block, which represents the conventional flat design, has the lowest average permeate flux at $3.38 \text{ g}/(\text{m}^2\text{s})$. However, looking only at changes in average permeate flux may not fully highlight the impact of the number of fins, as some differences are minor and expressed in decimal values. Therefore, the effect of the number of fins is further analysed by examining the percentage increase in average permeate flux compared to the conventional DCMD design shown in Figure 4.10 to better emphasize the impact.

According to Figure 4.10, the 9-fin block shows a 32.8% increase in average permeate flux, the highest among all the blocks. When the number of fins is reduced to 8, the percentage increase in average flux for the 8-fin block drops to 22.3%, indicating a steep decline of 10.5% compared to the 9-fin block. Further reducing the number of fins to 7 results in a steep decrease in percentage increase in average flux to only 5.5%, meaning the 7-fin block is only 5.5%

better than the flat block. Additionally, compared to the 9-fin and 8-fin blocks, the improvement in average permeate flux declines by 27.3% and 16.8%, respectively. This indicates that the number of fins significantly impacts the water production rate in the DCMD process, and selecting the optimal number of fins can enhance the performance of the DCMD module.

This is because the turbulence effect is important in a DCMD process, and the number of fins has a significant effect on the turbulence. With a higher number of fins in the channel design, the effective surface area increases, and the fluid flow within the feed channel becomes more turbulent due to the disruption of the flow pattern (Bahar, Hawlader and Ariff, 2015). This forces the fluid to move around the fins, creating eddies and increasing the mixing effect. Turbulence helps reduce the boundary layer thickness, which increases the heat and mass transfer rate between the feed and permeate sides of the membrane. This results in a higher vapor pressure difference and a more consistent temperature gradient across the membrane, leading to increased permeate flux. Therefore, when the number of fins decreases, the reduction in turbulence effect causes the block with fewer fins to behave almost like a flat block. This explains why blocks with fewer fins show results closer to those of the flat block and exhibit less improvement in average permeate flux compared to the flat block.

4.5 Conductivity Test for the DCMD Experiment

Table 4.7 lists the conductivity measured for the permeate solution before and after the experiment for all types of blocks, as well as the rejection rates for each block used in the DCMD system.

Table 4.7: Conductivity of the permeate solution before and after the experiment, with rejection rates for each block type.

Type	Permeate salinity, PPM		Permeate conductivity, $\mu\text{S}/\text{cm}$		Rejection Rate, %
	Initial	Final	Initial	Final	
Flat	2	3	3.1	4.7	99.99143
1	2	3	3.1	4.7	99.99143
2	2	3	3.1	4.7	99.99143
3	2	3	3.1	4.7	99.99143
4	2	2	3.1	3.1	99.99429
5	2	3	3.1	4.7	99.99143
6	2	3	3.1	4.7	99.99143
8-fin	2	3	3.1	4.7	99.99143
7-fin	2	3	3.1	4.7	99.99143

Based on Table 4.7, it can be observed that the initial permeate salinity measured was 2 ppm, and the final permeate salinity for the Type 4 block remained at 2 ppm. However, for the other blocks, the final permeate salinity increased slightly to 3 ppm. According to the Ministry of Health (2004), the maximum acceptable values in drinking water are 200 ppm for sodium and 250 ppm for chloride, as stated in the National Standard for Drinking Water Quality in Malaysia. Additionally, the initial permeate conductivity for all block types was 3.1 $\mu\text{S}/\text{cm}$, while the final permeate conductivity for all blocks, except for the Type 4 block, increased to 4.7 $\mu\text{S}/\text{cm}$. The final permeate conductivity for the Type 4 block remained at 3.1 $\mu\text{S}/\text{cm}$. According to the Department of Environment (2024), the electrical conductivity allowed for drinking water must be less than 1000 $\mu\text{S}/\text{cm}$, as stated in the National Water Quality Standards for Malaysia. Therefore, this indicates that the freshwater produced in the final permeate solution for all the blocks met Malaysia's drinking water standards and is safe for consumption.

Additionally, rejection rates in a DCMD system refer to the membrane's ability to block unwanted solutes, such as salt particles, in the feed solution from passing through to the permeate side. Therefore, a higher rejection

rate is crucial for producing high-quality, clean, and pure water from the feed solution, particularly in desalination processes. Based on Figure 4.16, the rejection rates for all blocks exceeded 99.99% and were very close to 100%. The Type 4 block had the highest rejection rate at 99.99429%, while the rest of the blocks had a rejection rate of 99.99143%. This indicates that the DCMD system used in this study is a highly efficient and reliable desalination system capable of providing freshwater from seawater.

4.6 Summary

In this chapter, it is demonstrated that channel designs with the same height-to-width ratio can still exhibit different performances when the channel height, the fin-to-channel width ratio, and the number of fins vary. Therefore, considering only the channel height-to-width ratio in designing a channel specifically to improve performance in the DCMD process might not be sufficient. This study demonstrates that selecting the correct channel height, fin-to-channel width ratio, and number of fins, which are close to the optimum levels, are also crucial parameters that must be considered to achieve the best performance from the DCMD module. By incorporating these three parameters in addition to the H/W ratio, the experiment identified a channel design that is close to the optimum. This near-optimal design features a channel height of 1.6 mm, a channel width of 2.6 mm, and a fin width of 2.13 mm, resulting in a fin-to-channel width ratio of 0.82 and a total of 9 fins. It provides the best performance results with an average permeate flux of 4.92 g/(m²s) and a 32.8% improvement in the DCMD process. Additionally, the conductivity of the final permeates from all block types used in this DCMD experiment met Malaysia's drinking water standards, and the rejection rate for the DCMD system across all blocks with different channel designs exceeded 99.99%. This indicates high efficiency in contaminant removal and demonstrates the reliability of the DCMD system. Therefore, the freshwater produced by this system is safe for consumption.

CHAPTER 5

CONCLUSIONS AND RECOMMENDATIONS

5.1 Conclusions

In conclusion, several factors influence the performance of a DCMD module. As discussed in the literature review, variations in these parameters can have different impacts on the DCMD process. Additionally, uncontrollable factors such as ambient laboratory temperature, the initial temperature of the distilled water used for the permeate solution, and room air velocity also affect performance. This study focused on modifying the channel design to investigate its effects on the DCMD process, as research in this area remains limited. Experiments were conducted using blocks with various channel designs under different temperature differences to explore the effects of specific parameters.

The study examined the influence of temperature difference on the permeate flux for all block types and assessed the impact of channel height and the fin-to-channel width ratio on average permeate flux and improvement in performance compared to the conventional flat block DCMD module. The aim was to identify the channel height, channel width, and fin width closest to the optimum for achieving the best performance results. Subsequently, with the channel height and width kept constant, the study reduced the number of fins on the block to assess the effect of the number of fins on DCMD performance.

Analysis of the experimental data revealed that a higher temperature difference results in a higher permeate flux for all block types. Increasing channel height also led to higher average permeate flux and improved performance, but exceeding the optimum channel height caused a decline. Similarly, decreasing the fin-to-channel width ratio resulted in higher average permeate flux and improvement in performance, but reducing the ratio beyond the optimum led to a decline. Additionally, a higher number of fins provided better performance compared to blocks with fewer fins.

The analysis identified that the channel design closest to optimum, which provided the best performance, featured a channel height of 1.6 mm, a channel width of 2.6 mm, a fin width of 2.13 mm, and a total of 9 fins. This

design achieved an average permeate flux of 4.92 g/(m²s) and a 32.8% improvement over the conventional flat block DCMD module. Furthermore, all block types used in the DCMD module produced freshwater that met Malaysia's drinking water standards and achieved a rejection rate of over 99.99%, demonstrating that the DCMD system is both efficient and reliable for producing freshwater from seawater.

5.2 Recommendations for future work

The channel design used and studied in this research is limited to the rectangular channel design due to the limitations of the workshop tools. However, many other channel designs could be explored other than the rectangular shape. Future research can maintain the channel height and width that give higher water production rates, as identified in this study, while modifying the channel shape to zigzag or wavy patterns. Zigzag and wavy channels, being non-linear, can reduce the formation of stagnation zones and improve turbulence. Additionally, future studies can add the extra feature of higher surface roughness in the channels and fins in the finned block, as rougher surfaces can enhance turbulence, which is useful to increase the performance of the DCMD process. Therefore, future research should focus on channel designs that further improve turbulence to enhance DCMD performance. Another recommendation is to conduct experiments in a controlled environment to minimize the effects of external variables, such as ambient lab temperature and air velocity, to achieve more consistent and reliable results.

REFERENCES

- Ahmad, H.M., Khalifa, A.E. and Antar, M.A., 2015. Water desalination using direct contact membrane distillation system. *Volume 6A: Energy*, [e-journal]. <https://doi.org/10.1115/imece2015-50171>.
- Ali, K., Kharraz, J.A., Khatab, M.Z., Hasanm S.W. and Ali, M.I.H, 2024. Numerical investigation of multiple channels module for enhanced water production in membrane distillation. *Desalination*, [e-journal] 586, p. 117886. <https://doi.org/10.1016/j.desal.2024.117886>.
- Ashoor, B.B., Mansour, S., Giwa, A., Dufour, A. and Hasan, S.W., 2016. Principles and applications of direct contact membrane distillation (DCMD): A comprehensive review. *Desalination*, [e-journal] 398, pp. 222–246. <http://dx.doi.org/10.1016/j.desal.2016.07.043>.
- ASM International, 2023. *Aluminum and Aluminum Alloys Subject Guide*. [online] ASM International. Available at: <<https://www.asminternational.org/aluminum-and-aluminum-alloys-subject-guide/#:~:text=Aluminum%20and%20aluminum%20alloys%20have,strength%2C%20and%20relatively%20low%20cost.>> [Accessed 5 September 2024].
- Bahar, R., Hawlader, M.N.A. and Ariff, T.F., 2015. Channeled coolant plate: A new method to enhance freshwater production from an air gap membrane distillation (AGMD) Desalination Unit. *Desalination*, [e-journal] 359, pp. 71–81. <http://dx.doi.org/10.1016/j.desal.2014.12.031>.
- Chang, H., Ho, C. and Hsu, J., 2016. Analysis of heat transfer coefficients in direct contact membrane distillation modules using CFD Simulation. *Journal of Applied Science and Engineering*, [e-journal] 19(2), pp. 197–206. <https://doi.org/10.6180/jase.2016.19.2.10>.
- Chang, H., Hsu, J., Chang, C. and Ho, C., 2015. CFD simulation of direct contact membrane distillation modules with rough surface channels. *Energy Procedia*, [e-journal] 75, pp. 3083–3090. 10.1016/j.egypro.2015.07.634.
- Chang, H., Hsu, J., Chang, C. and Ho, C., 2015. CFD study of heat transfer enhanced membrane distillation using spacer-filled channels. *Energy Procedia*, [e-journal] 75, pp. 3213–3219. 10.1016/j.egypro.2015.07.680.
- Chang, H., Hsu, J., Chang, C., Ho, C. and Cheng, T., 2017. Simulation study of transfer characteristics for spacer-filled membrane distillation desalination modules. *Applied Energy*, [e-journal] 185, pp. 2045–2057. <http://dx.doi.org/10.1016/j.apenergy.2015.12.030>.
- Cheong, H.P. 2024. *Study on the performance of direct contact membrane distillation coupled with channels*. BEng. Universiti Tunku Abdul Rahman.

Department of Environment, 2024. *National Water Quality Standards for Malaysia*. [pdf] Malaysia: Department of Environment. Available at: < <https://doe.gov.my/wp-content/uploads/2021/11/Standard-Kualiti-Air-Kebangsaan.pdf> > [Accessed 5 September 2024].

Ho, C., Chang, H., Chang, C. and Huang, C., 2013. Theoretical and experimental studies of flux enhancement with roughened surface in direct contact membrane distillation desalination. *Journal of Membrane Science*, [e-journal] 433, pp. 160–166. <http://dx.doi.org/10.1016/j.memsci.2012.12.044>.

Ho, C., Huang, C., Tsai, F. and Chen, W., 2014. Performance improvement on distillate flux of countercurrent-flow direct contact membrane distillation systems. *Desalination*, [e-journal] 338, pp. 26–32. <http://dx.doi.org/10.1016/j.desal.2014.01.023>.

Jimenez-Hornero, F.J., Zhang, X.X., Giraldez, J.V. and Laguna, A.M., 2008. Numerical Study of the Transition Regime between the Skimming and Wake Interference Flows in a Water Flume by Using the Lattice-Model Approach. *Journal of Hydraulic Engineering*, [e-journal] 134(2), pp. 274–279. [https://doi.org/10.1061/\(asce\)0733-9429\(2008\)134:2\(274\)](https://doi.org/10.1061/(asce)0733-9429(2008)134:2(274)).

Kim, Y., Francis, L., Lee, J., Ham, M. and Ghaffour, N., 2018. Effect of non-woven net spacer on a direct contact membrane distillation performance: Experimental and theoretical studies. *Journal of Membrane Science*, [e-journal] 564, pp. 193–203. <https://doi.org/10.1016/j.memsci.2018.07.019>.

Ministry of Health, 2004. *National Standard for Drinking Water Quality*. Malaysia: Ministry of Health.

Momeni, M., Kargari, A., Dadvar, M. and Jafari, A., 2024. 3D-CFD simulation of hollow fiber direct contact membrane distillation module: Effect of module and fibers geometries on hydrodynamics, mass, and heat transfer. *Desalination*, [e-journal] 576, p. 117321. <https://doi.org/10.1016/j.desal.2024.117321>.

Ni, W., Li, Y., Zhang, G. and Du, X., 2022. Study of spacer structure on the enhancement of heat and mass transfer in direct contact membrane distillation modules. *Desalination*, [e-journal] 530, p. 115617. <https://doi.org/10.1016/j.desal.2022.115617>.

Park, D.J., Norouzi, E. and Park, C., 2019. Experimentally-validated computational simulation of direct contact membrane distillation performance. *International Journal of Heat and Mass Transfer*, [e-journal] 129, pp. 1031–1042. <https://doi.org/10.1016/j.ijheatmasstransfer.2018.10.035>.

Rabie, M., Elkady, M.F. and El-Shazly, A.H., 2021. Effect of channel height on the overall performance of direct contact membrane distillation. *Applied Thermal Engineering*, [e-journal] 196, p. 117262. <https://doi.org/10.1016/j.applthermaleng.2021.117262>.

- Sampaio, P.A.B., Alves, L.F.R., and Moreira, M.L., 2023. Electricity and water cogeneration using a small PWR of 75 MW (th) coupled to a DCMD desalination plant with heat recovery. *Nuclear Engineering and Design*, [e-journal] 415, p. 112658. <https://doi.org/10.1016/j.nucengdes.2023.112658>.
- Shirazi, M.M.A. and Kargari, A., 2015. A review on applications of membrane distillation (MD) process for wastewater treatment. *Journal of Membrane Science and Research*, 1, pp. 101-112.
- Swaidan, B., Ali, M.I.H., Ali, K., Al-Rub, R.K.A. and Arafat, H.A., 2024. A computational fluid dynamics study on TPMS-based spacers in direct contact membrane distillation modules. *Desalination*, [e-journal] 579, p. 117476. <https://doi.org/10.1016/j.desal.2024.117476>.
- Taamneh, Y. and Bataineh, K., 2017. Improving the performance of direct contact membrane distillation utilizing spacer-filled channel. *Desalination*, [e-journal] 408, pp. 25–35. <http://dx.doi.org/10.1016/j.desal.2017.01.004>.
- Ve, Q.L., Rahaoui, K., Bawahab, M., Faqeha, H., Date, A., Faghih, A. and Akbarzadeh, A., 2019. An experimental heat transfer investigation of using spacer in direct contact membrane distillation. *Energy Procedia*, [e-journal] 160, pp. 223–230. [10.1016/j.egypro.2019.02.140](https://doi.org/10.1016/j.egypro.2019.02.140).
- World Health Organisation, 2023. *Drinking-water*. [online] World Health Organization. Available at: <https://www.who.int/news-room/factsheets/detail/drinking-water> [Accessed 20 April 2024].
- Xie, S., Liang, Z., Zhang, J., Zhang, L., Wang, Y. and Ding, H., 2019. Numerical investigation on flow and heat transfer in dimpled tube with Teardrop Dimples. *International Journal of Heat and Mass Transfer*, [e-journal] 134(2), pp. 713–723. <https://doi.org/10.1016/j.ijheatmasstransfer.2018.11.112>.
- Yadav, A., Singh, C.P., Patel, R.V., Kumar, A. and Labhsetwar, P.K., 2022. Investigations on the effect of spacer in direct contact and air gap membrane distillation using computational fluid dynamics. *Colloids and Surfaces A: Physicochemical and Engineering Aspects*, [e-journal] 654, p. 130111. <https://doi.org/10.1016/j.colsurfa.2022.130111>.
- Zare, S. and Kargari, A., 2022. CFD simulation and optimization of an energy-efficient direct contact membrane distillation (DCMD) desalination system. *Chemical Engineering Research and Design*, [e-journal] 188, pp. 655–667. <https://doi.org/10.1016/j.cherd.2022.10.001>.
- Zhuang, N., Tan, S., Yuan, H. and Yang, B., 2017. Flow resistance of low-frequency pulsatile turbulent flow in mini-channels. *International Journal of Heat and Fluid Flow*, [e-journal] 65, pp. 21–32. <http://dx.doi.org/10.1016/j.ijheatfluidflow.2017.03.005>.

APPENDICES

Appendix A: Experimental Data

Table A-1: Experimental data for Flat Block.

Time (min)	Temperature (°C)			Weight Increment (g)	Permeate Flux, g/(m ² s)
	Feed, T_f	Permeate, T_p	Difference, ($T_f - T_p$)		
0	50.1	24.4	25.7	-	-
10	49.5	25.9	23.6	4.0	4.17
20	49.7	27.6	22.1	3.8	3.96
30	49.6	28.9	20.7	3.6	3.75
40	49.5	30.0	19.5	3.4	3.54
50	50.0	30.9	19.1	3.2	3.33
60	49.9	31.9	18.0	3.3	3.44
70	50.2	32.6	17.6	3.2	3.33
80	50.3	33.2	17.1	3.1	3.23
90	50.6	33.7	16.9	3.2	3.33
100	50.1	34.1	16.0	3.0	3.13
110	50.1	34.5	15.6	2.8	2.92
120	50.2	34.8	15.4	2.9	3.02
130	50.0	35.1	14.9	2.7	2.81
Average				3.3	3.17

The results from Table A-1 are shown in Figures A-1 and A-2.

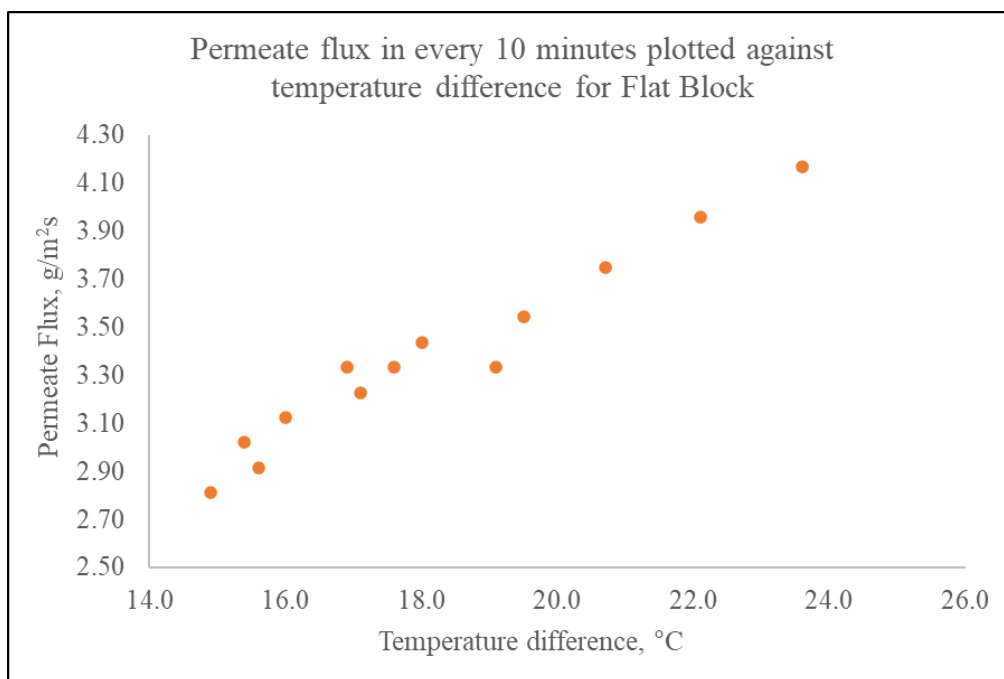


Figure A-1: Permeate flux in every 10 minutes plotted against the temperature difference for flat block.

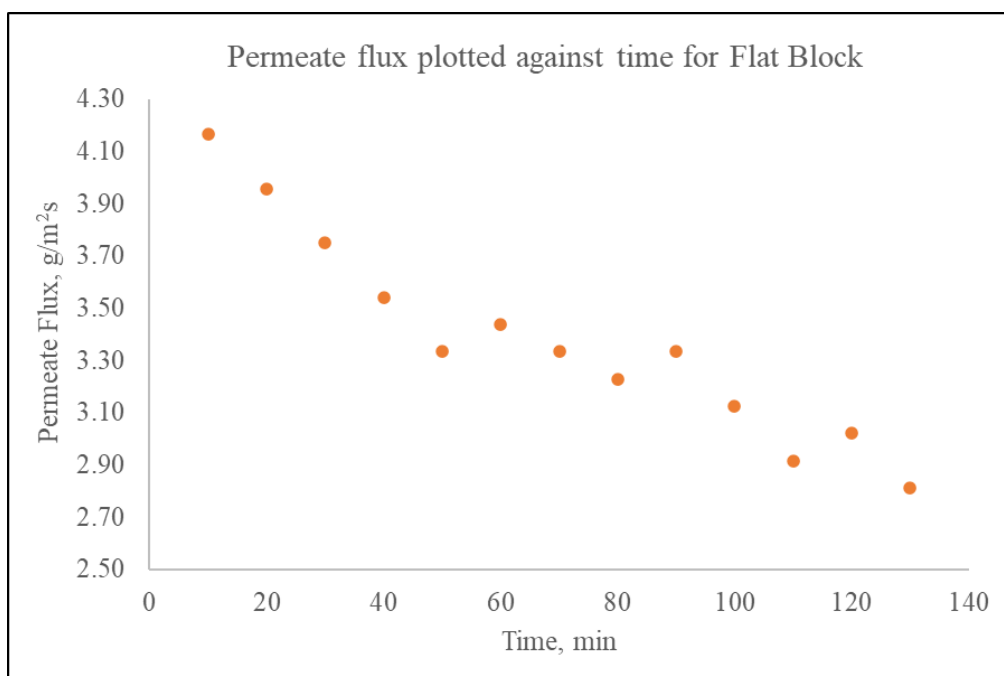


Figure A-2: Permeate flux plotted against time for flat block.

Table A-2: Experimental data for Type 1 Block.

Time (min)	Temperature (°C)			Weight Increment (g)	Permeate Flux, g/(m ² s)
	Feed, T_f	Permeate, T_p	Difference, ($T_f - T_p$)		
0	50.2	25.6	24.6	-	-
10	48.9	27.0	21.9	4.6	4.79
20	49.6	28.3	21.3	4.5	4.69
30	49.9	29.7	20.2	4.4	4.58
40	49.9	30.7	19.2	4.2	4.37
50	50.0	31.7	18.3	4.0	4.17
60	50.2	32.5	17.7	3.8	3.96
70	50.3	33.1	17.2	3.6	3.75
80	50.5	33.7	16.8	3.2	3.33
90	50.7	34.2	16.5	3.5	3.65
100	50.5	34.6	15.9	3.4	3.54
110	50.4	34.9	15.5	3.3	3.44
120	50.5	35.2	15.3	3.5	3.65
130	50.5	35.5	15.0	3.4	3.54
Average				3.8	3.67

The results from Table A-2 are shown in Figures A-3 and A-4.

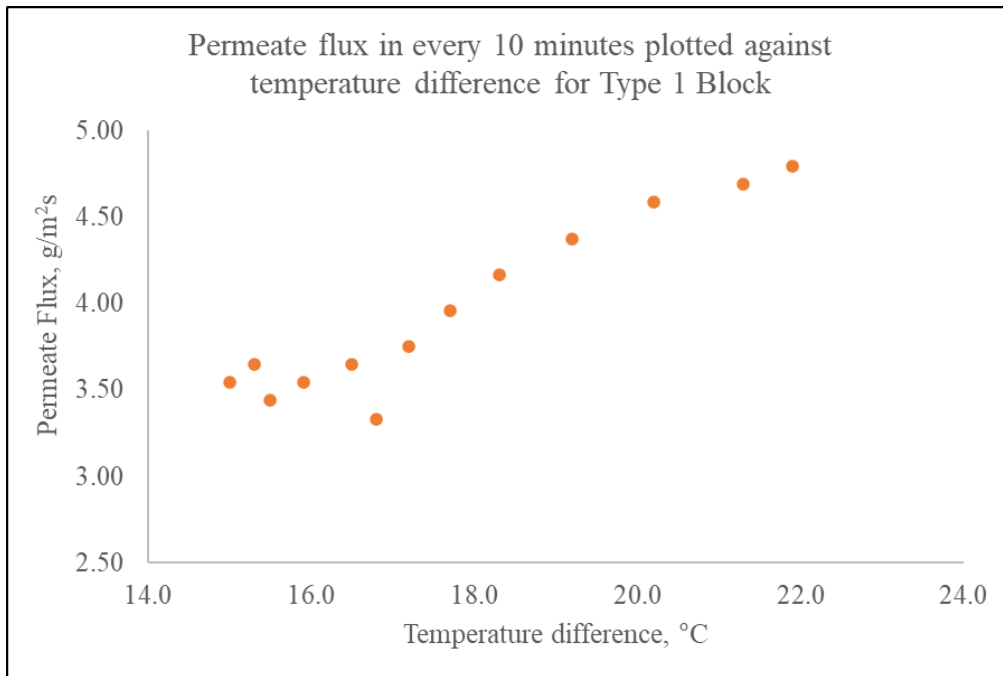


Figure A-3: Permeate flux in every 10 minutes plotted against the temperature difference for type 1 block.

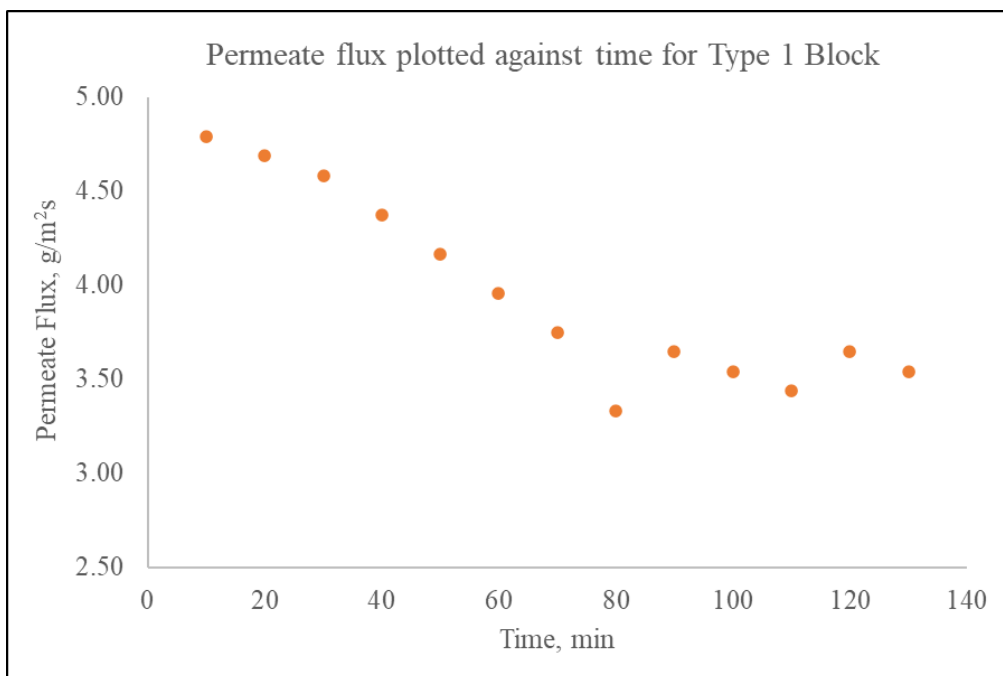


Figure A-4: Permeate flux plotted against time for type 1 block.

Table A-3: Experimental data for Type 2 Block.

Time (min)	Temperature (°C)			Weight Increment (g)	Permeate Flux, g/(m ² s)
	Feed, T_f	Permeate, T_p	Difference, (T_f-T_p)		
0	50.8	25.1	25.7	-	-
10	49.6	26.7	22.9	5.0	5.21
20	49.7	28.4	21.3	4.6	4.79
30	49.8	29.6	20.2	4.3	4.48
40	49.9	30.7	19.2	4.3	4.48
50	49.9	31.8	18.1	4.1	4.27
60	50.3	32.6	17.7	3.9	4.06
70	50.6	33.3	17.3	4.1	4.27
80	50.8	34.0	16.8	4.0	4.17
90	50.6	34.7	15.9	3.8	3.96
100	50.4	35.0	15.4	3.7	3.85
110	50.6	35.3	15.3	3.6	3.75
120	50.5	35.6	14.9	3.4	3.54
130	50.6	35.8	14.8	3.4	3.54
Average				4.0	3.94

The results from Table A-3 are shown in Figures A-5 and A-6.

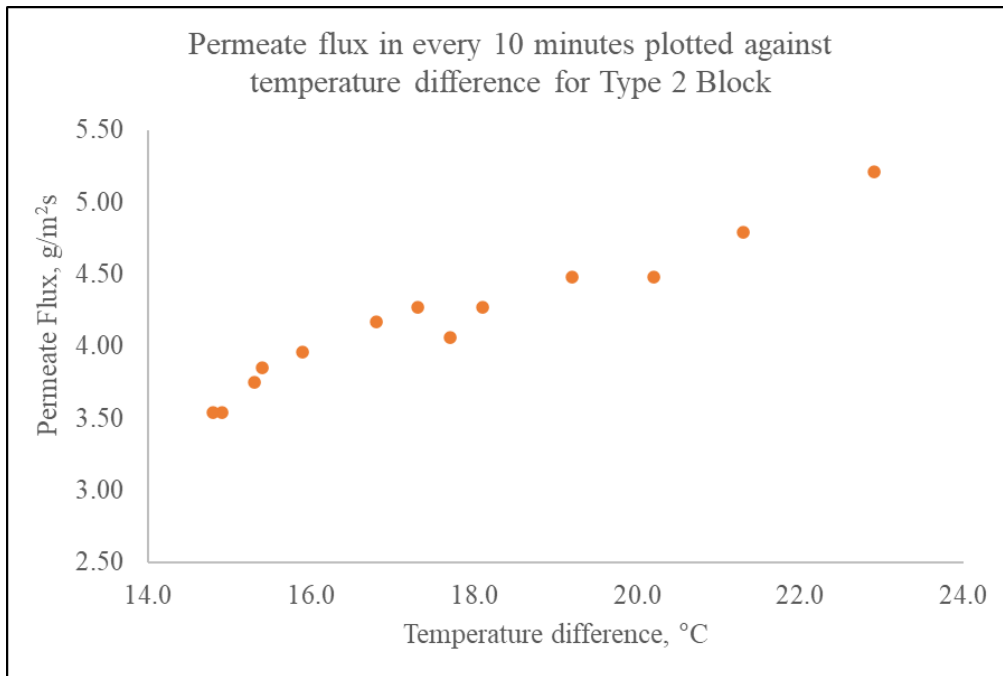


Figure A-5: Permeate flux in every 10 minutes plotted against the temperature difference for type 2 block.

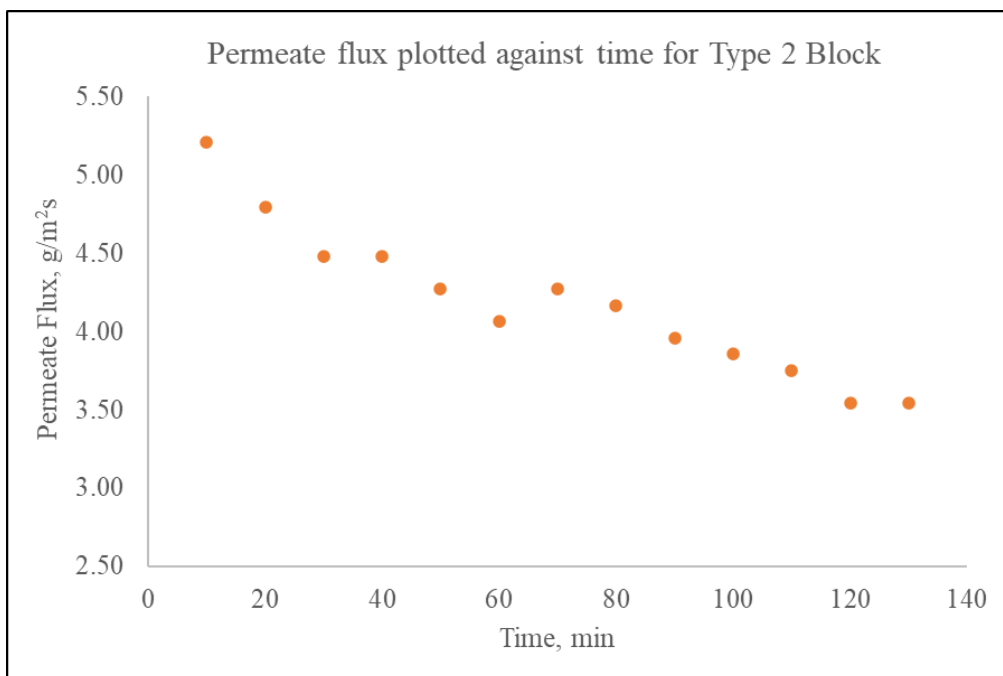


Figure A-6: Permeate flux plotted against time for type 2 block.

Table A-4: Experimental data for Type 3 Block.

Time (min)	Temperature (°C)			Weight Increment (g)	Permeate Flux, g/(m ² s)
	Feed, T_f	Permeate, T_p	Difference, ($T_f - T_p$)		
0	50.6	24.9	25.7	-	-
10	49.0	26.2	22.8	5.8	6.04
20	49.7	28.1	21.6	5.5	5.73
30	50.0	29.5	20.5	5.3	5.52
40	50.2	30.6	19.6	5.1	5.31
50	50.3	31.5	18.8	4.2	4.37
60	50.5	32.6	17.9	4.1	4.27
70	50.6	33.5	17.1	4.1	4.27
80	50.9	33.9	17.0	3.8	3.96
90	50.6	34.6	16.0	4.0	4.17
100	50.6	35.0	15.6	3.9	4.06
110	50.4	35.5	14.9	3.6	3.75
120	50.4	35.8	14.6	3.6	3.75
130	50.8	36.0	14.8	3.5	3.65
Average				4.3	4.03

The results from Table A-4 are shown in Figures A-7 and A-8.

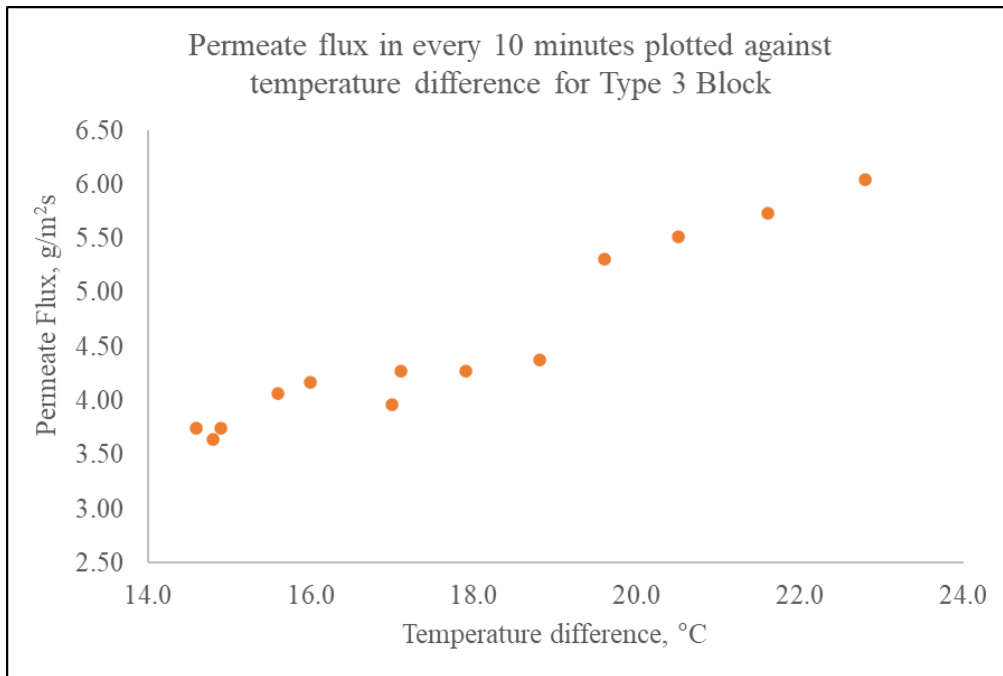


Figure A-7: Permeate flux in every 10 minutes plotted against the temperature difference for type 3 block.

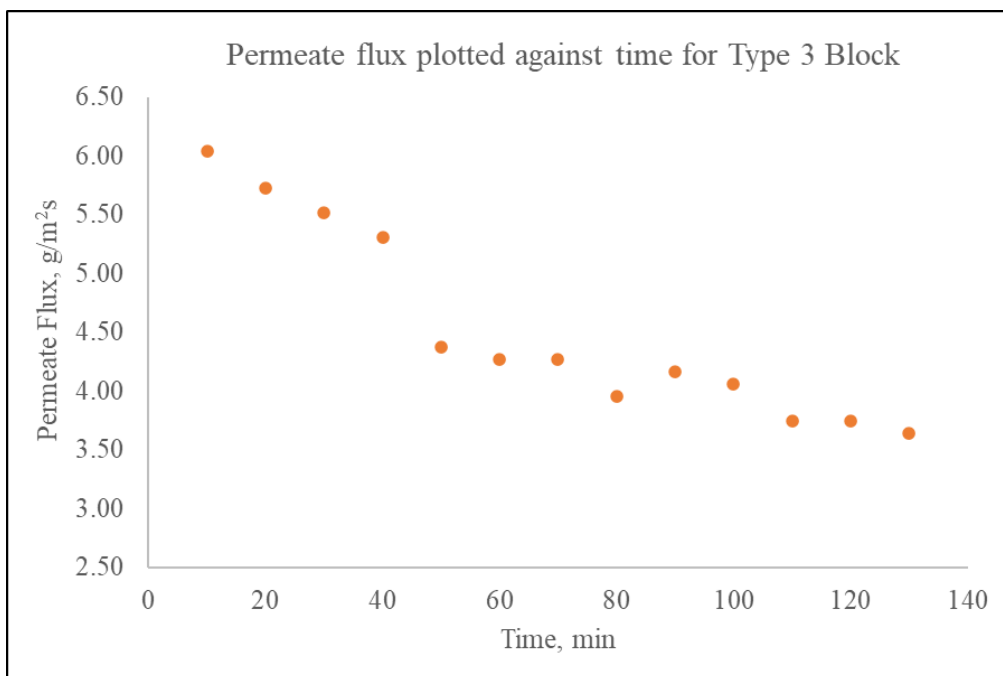


Figure A-8: Permeate flux plotted against time for type 3 block.

Table A-5: Experimental data for Type 4 Block.

Time (min)	Temperature (°C)			Weight Increment (g)	Permeate Flux, g/(m ² s)
	Feed, T_f	Permeate, T_p	Difference, ($T_f - T_p$)		
0	51.3	24.9	26.4	-	-
10	49.0	26.6	22.4	8.0	8.33
20	49.3	28.1	21.2	6.6	6.88
30	49.6	29.4	20.2	5.4	5.62
40	49.8	30.5	19.3	5.0	5.21
50	50.1	31.5	18.6	4.4	4.58
60	50.3	32.3	18.0	4.6	4.79
70	50.5	32.9	17.6	4.2	4.37
80	50.8	33.6	17.2	4.1	4.27
90	51.0	34.1	16.9	4.1	4.27
100	50.3	34.6	15.7	3.9	4.06
110	50.6	35.1	15.5	3.8	3.96
120	50.6	35.4	15.2	3.6	3.75
130	50.8	35.6	15.2	3.7	3.85
Average				4.7	4.21

The results from Table A-5 are shown in Figures A-9 and A-10.

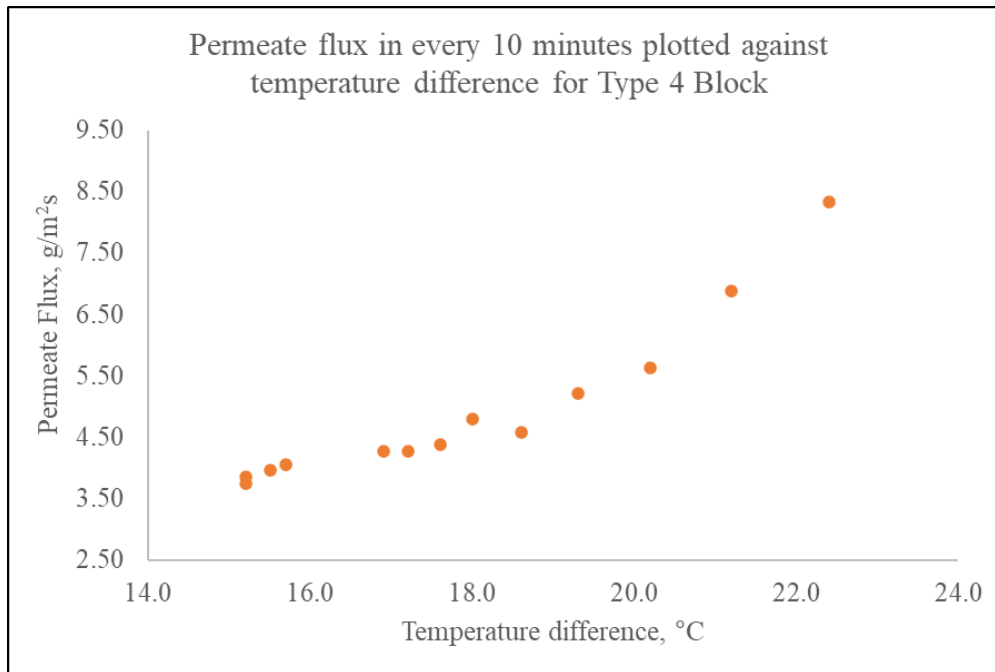


Figure A-9: Permeate flux in every 10 minutes plotted against the temperature difference for type 4 block.

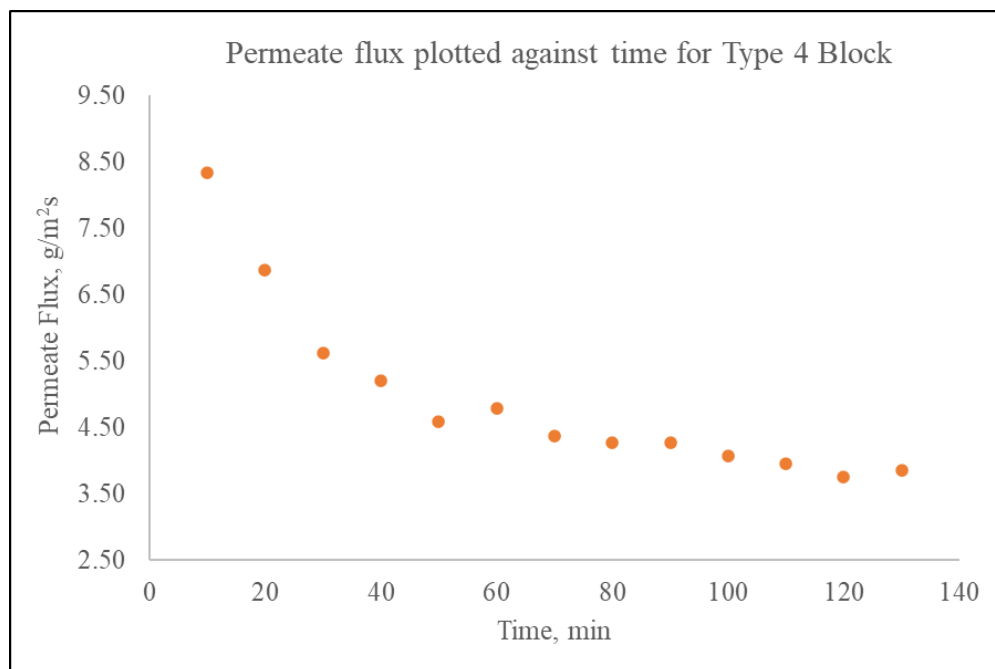


Figure A-10: Permeate flux plotted against time for type 4 block.

Table A-6: Experimental data for Type 5 Block.

Time (min)	Temperature (°C)			Weight Increment (g)	Permeate Flux, g/(m ² s)
	Feed, T_f	Permeate, T_p	Difference, ($T_f - T_p$)		
0	49.7	24.8	24.9	-	-
10	48.5	26.5	22.0	5.5	5.73
20	49.6	28.0	21.6	5.2	5.42
30	48.9	29.4	19.5	4.2	4.37
40	49	30.3	18.7	4.5	4.69
50	49.7	31.3	18.4	4.1	4.27
60	50	32.3	17.7	4.3	4.48
70	50.3	32.8	17.5	3.5	3.65
80	50.5	33.5	17.0	3.8	3.96
90	50.4	34.0	16.4	3.7	3.85
100	50.4	34.5	15.9	3.7	3.85
110	50.5	34.9	15.6	3.6	3.75
120	50.6	35.3	15.3	3.5	3.65
130	50.6	35.5	15.1	3.4	3.54
Average				4.1	3.89

The results from Table A-6 are shown in Figures A-11 and A-12.

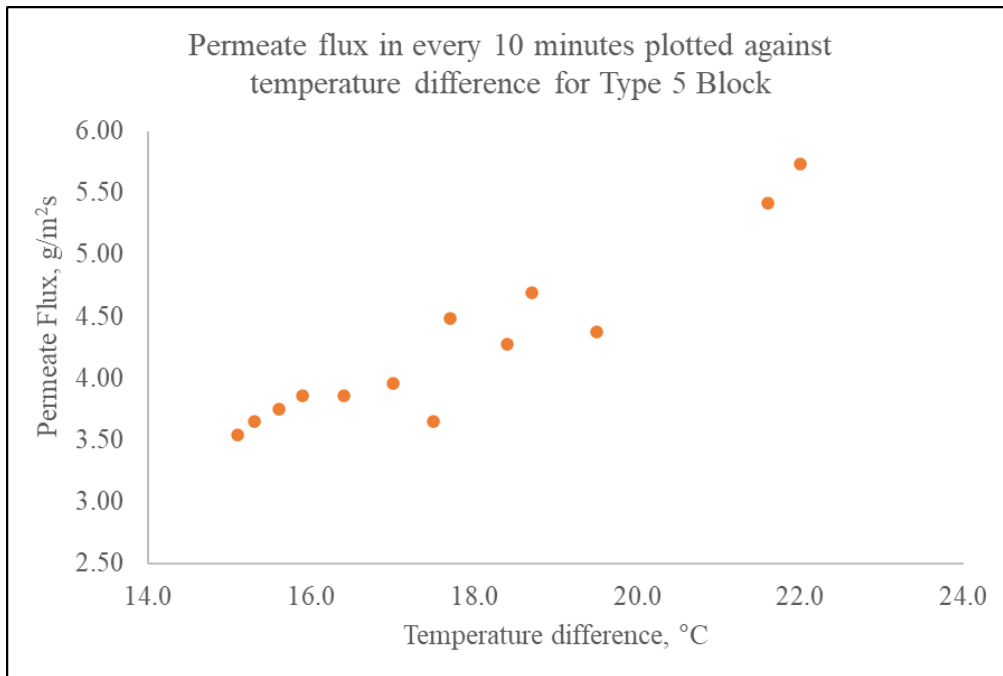


Figure A-11: Permeate flux in every 10 minutes plotted against the temperature difference for type 5 block.

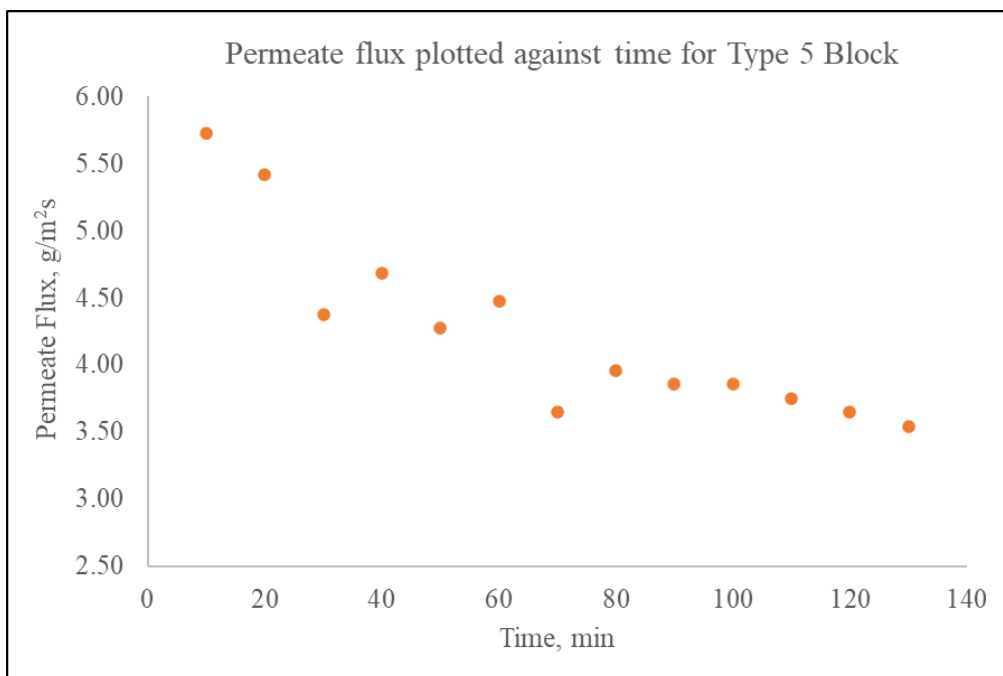


Figure A-12: Permeate flux plotted against time for type 5 block.

Table A-7: Experimental data for Type 6 Block.

Time (min)	Temperature (°C)			Weight Increment (g)	Permeate Flux, g/(m ² s)
	Feed, T_f	Permeate, T_p	Difference, $(T_f - T_p)$		
0	49.7	25.9	23.8	-	-
10	49.0	27.3	21.7	4.8	5.00
20	49.8	28.9	20.9	4.3	4.48
30	49.8	30.1	19.7	4.0	4.17
40	49.9	31.2	18.7	4.0	4.17
50	50.2	31.8	18.4	3.7	3.85
60	50.5	32.8	17.7	3.6	3.75
70	50.6	33.5	17.1	3.6	3.75
80	50.7	34.1	16.6	3.5	3.65
90	50.4	34.6	15.8	3.3	3.44
100	50.5	35.0	15.5	3.4	3.54
110	50.4	35.5	14.9	3.2	3.33
120	50.7	35.7	15.0	3.3	3.44
130	50.5	36.0	14.5	3.1	3.23
Average				3.7	3.55

The results from Table A-7 are shown in Figures A-13 and A-14.

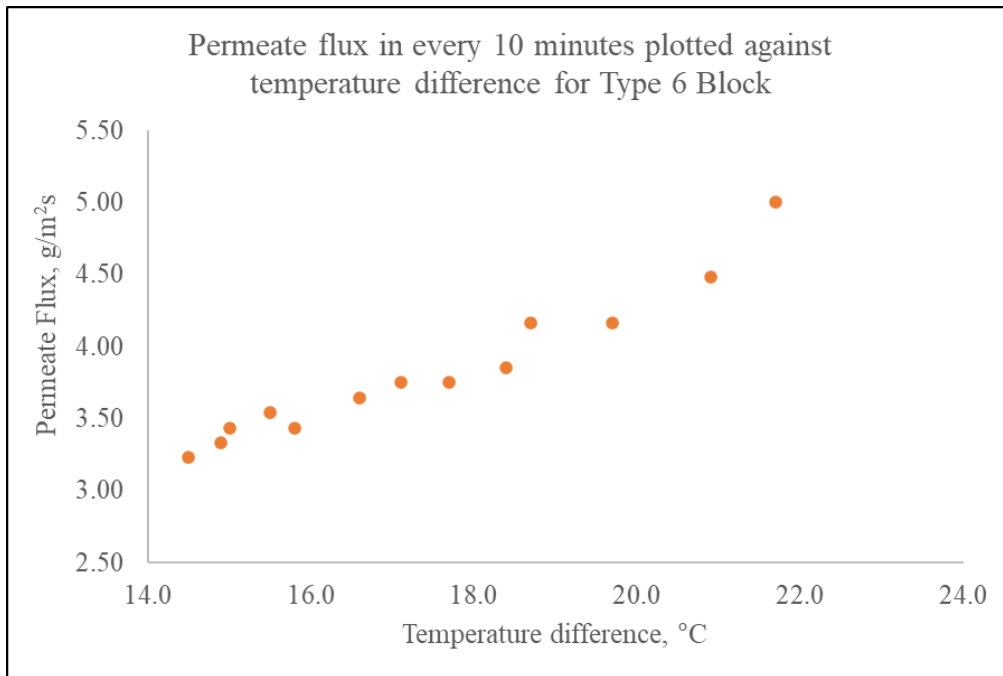


Figure A-13: Permeate flux in every 10 minutes plotted against the temperature difference for type 6 block.

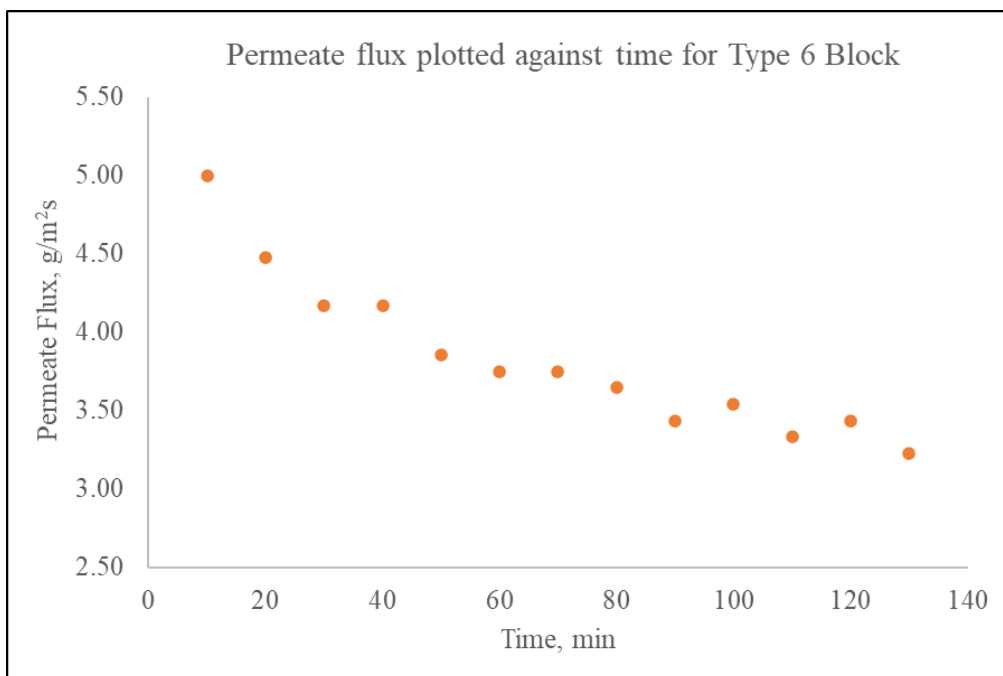


Figure A-14: Permeate flux plotted against time for type 6 block.

Table A-8: Experimental data for 8-fin Block.

Time (min)	Temperature (°C)			Weight Increment (g)	Permeate Flux, g/(m ² s)
	Feed, T_f	Permeate, T_p	Difference, ($T_f - T_p$)		
0	49.9	25.7	24.2	-	-
10	49.1	26.9	22.2	5.1	5.31
20	49.7	28.4	21.3	4.6	4.79
30	50.1	29.6	20.5	4.3	4.48
40	50.3	30.7	19.6	4.1	4.27
50	50.8	31.7	19.1	4.2	4.37
60	50.6	32.3	18.3	3.9	4.06
70	50.3	33.1	17.2	3.9	4.06
80	50.3	33.6	16.7	3.7	3.85
90	50.4	34.1	16.3	3.8	3.96
100	50.5	34.5	16.0	3.5	3.65
110	50.3	34.9	15.4	3.6	3.75
120	50.3	35.1	15.2	3.6	3.75
130	50.2	35.4	14.8	3.3	3.44
Average				4.0	3.88

The results from Table A-8 are shown in Figures A-15 and A-16.

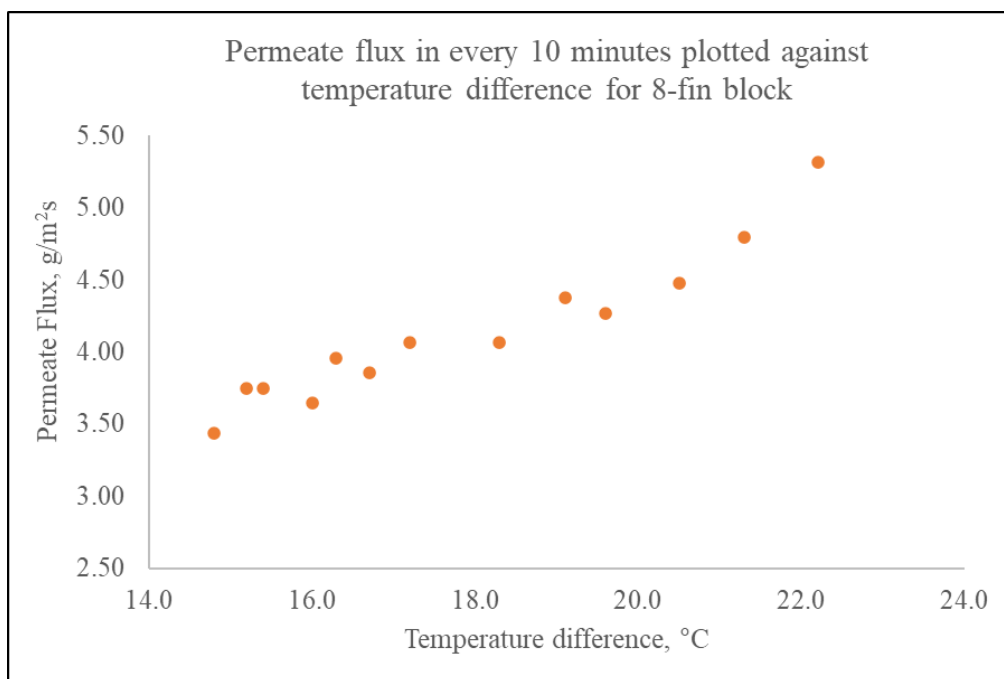


Figure A-15: Permeate flux in every 10 minutes plotted against the temperature difference for 8-fin block.

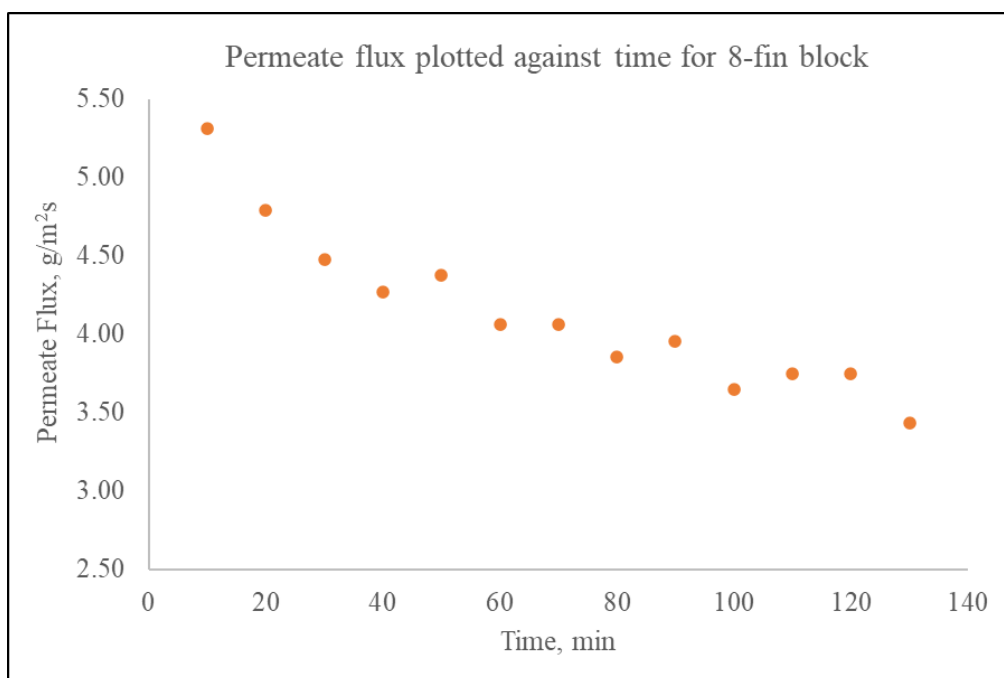


Figure A-16: Permeate flux plotted against time for 8-fin block.

Table A-9: Experimental data for 7-fin Block.

Time (min)	Temperature (°C)			Weight Increment (g)	Permeate Flux, g/(m ² s)
	Feed, T_f	Permeate, T_p	Difference, ($T_f - T_p$)		
0	49.8	24.4	25.4	-	-
10	49.4	26.0	23.4	4.4	4.58
20	49.9	27.7	22.2	4.1	4.27
30	50.1	29.1	21.0	3.6	3.75
40	50.2	30.3	19.9	3.5	3.65
50	50.5	31.2	19.3	3.3	3.44
60	50.3	32.1	18.2	3.4	3.54
70	50.5	33.1	17.4	3.1	3.23
80	50.6	33.7	16.9	3.2	3.33
90	50.6	34.2	16.4	3.3	3.44
100	50.5	34.7	15.8	3.0	3.13
110	50.6	35.1	15.5	3.4	3.54
120	50.4	35.4	15.0	3.2	3.33
130	50.3	35.7	14.6	3.0	3.13
Average				3.4	3.34

The results from Table A-9 are shown in Figures A-17 and A-18.

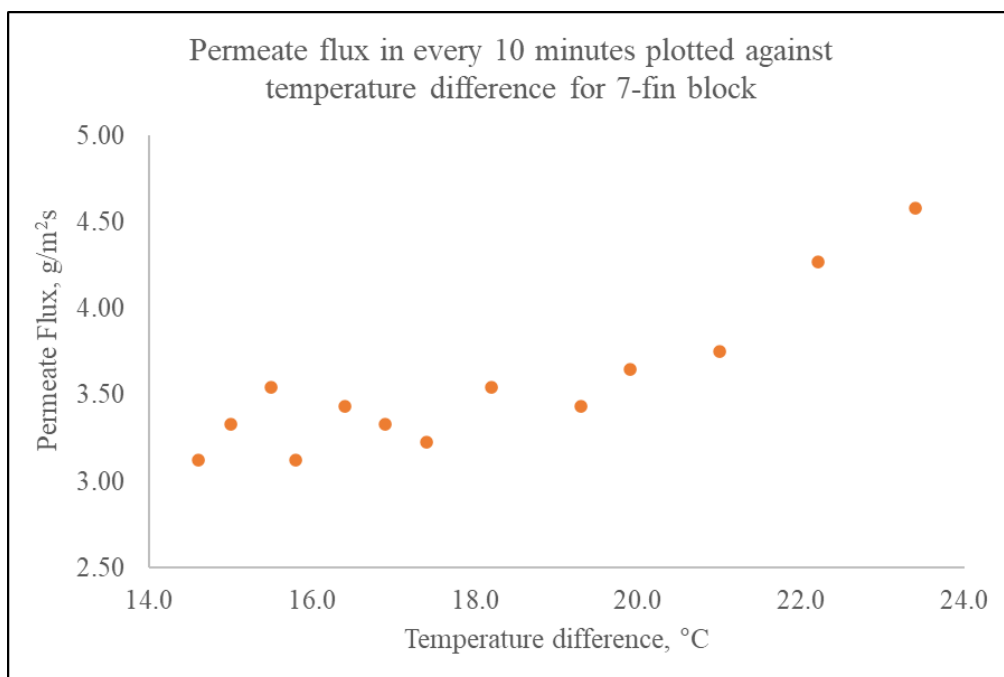


Figure A-17: Permeate flux in every 10 minutes plotted against the temperature difference for 7-fin block.

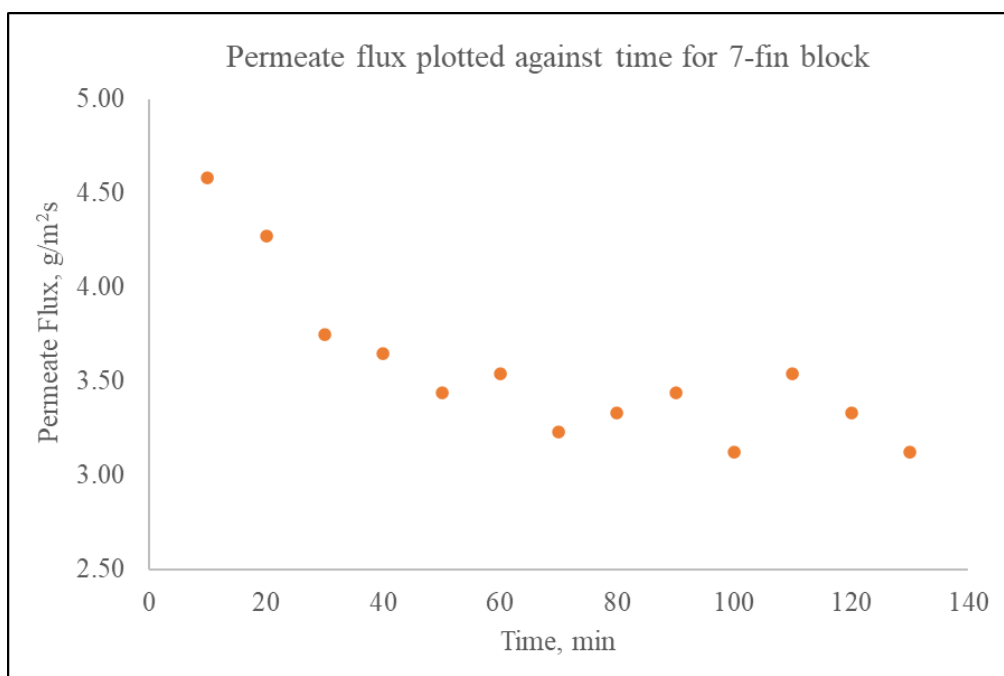


Figure A-18: Permeate flux plotted against time for 7-fin block.